Journal of Medicinal Chemistry

Article

Validation of Phosphodiesterase-10 as a Novel Target for Pulmonary Arterial Hypertension via Highly Selective and Subnanomolar Inhibitors

Yi-You Huang, Yanfa Yu, Chen Zhang, Yiping Chen, Qian Zhou, Zhuoming Li, Sihang Zhou, Zhe Li, Lei Guo, Deyan Wu, Yinuo Wu, and Hai-Bin Luo

J. Med. Chem., **Just Accepted Manuscript** • DOI: 10.1021/acs.jmedchem.9b00224 • Publication Date (Web): 19 Mar 2019

Just Accepted

ACS Publications

is published by the American Chemical Society. 1155 Sixteenth Street N.W., Washington, DC 20036

Validation of Phosphodiesterase-10 as a Novel Target for Pulmonary Arterial Hypertension *via* Highly Selective and Subnanomolar Inhibitors

Yi-You Huang‖, Yan-Fa Yu‖, Chen Zhang‖, Yiping Chen, Qian Zhou, Zhuoming Li, Sihang Zhou, Zhe Li, Lei Guo, Deyan Wu*, Yinuo Wu*, and Hai-Bin Luo*

School of Pharmaceutical Sciences, Sun Yat-sen University, Guangzhou 510006, China

■ ABSTRACT

Pulmonary arterial hypertension (PAH) causes pathological increase in pulmonary vascular resistance, leading to right-heart failure and eventual death. Previously, phosphodiesterase-10 (PDE10) was reported to be a promising target for PAH based on the studies with a non-selective PDE inhibitor papaverine, but little progress has been made to confirm the practical application of PDE10 inhibitors. To validate whether PAH is ameliorated by PDE10 inhibition rather than other PDE isoforms, here we report an integrated strategy to discover highly selective PDE10 inhibitors as chemical probes. Structural optimization resulted in a PDE10 inhibitor **2b** with subnanomolar affinity and good selectivity of > 45 000-fold against other PDEs. The cocrystal structure of the PDE10-**2b** complex revealed an important H-bond interaction between **2b** and Tyr693. Finally, compound **2b** significantly decreased the arterial pressure in PAH rats and thus validated the potential of PDE10 as a novel anti-PAH target. These findings suggest that PDE10 inhibition may be a viable treatment option for PAH.

■ INTRODUCTION

Phosphodiesterases (PDEs) are important enzymes that hydrolyze the second messengers cyclic adenosine monophosphate (cAMP) and cyclic guanosine monophosphate (cGMP).[1] Due to the critical roles of cAMP and cGMP in physiologic processes, PDEs have attracted wide attention of researchers as drug targets for treatment of human diseases. Till now, 11 selective PDEs inhibitors have been approved in clinic, such as the PDE5 inhibitors of sildenafil and tadalafil, which are the treatments for erectile dysfunction and pulmonary arterial hypertension (PAH).[2] In addition to the high expression

in the lung, PDE10 is expressed at high levels in the medium spiny neurons of the striatum and thought to modulate the downstream dopaminergic and glutamatergic signaling pathways.[3] As a result, several PDE10 inhibitors have entered clinical Phase I/II trials for the treatment of central nervous system (CNS) disorders.[4-8]

PAH is a debilitating and progressive disease of the pulmonary vasculature and causes right ventricular failure and eventual death. Although significant advances in understanding of the pathobiology of PAH have brought the development of several therapeutics against this disease, a clear unmet medical need exists.[9,10] Recently, PDE10 was reported to be a promising target for treatment of PAH based on studies with a non-selective inhibitor papaverine.[11] However, little progresses has been made to confirm PDE10 as an anti-PAH target. Since the loss of nitric oxide (NO)- and PGI_2-driven cGMP and cAMP signaling is an important hallmark of PAH, agents such as PDE5 inhibitors sildenafil/tadalafil (elevating cGMP level) and iloprost (elevating cAMP signaling) have been proven to be one of effective PAH therapeutics.[12] In general, PDE10 inhibitors might augment both cAMP and cGMP signaling[13,14] and potentially exert additive effects, suggesting that PDE10 is an appealing target that potentially opens a new avenue to develop effective anti-PAH therapeutics.

Besides PDE10 and PDE5, several other PDE isoforms including PDE1, PDE2, PDE3 and PDE4, are also involved in the pathological mechanism of PAH, as indicated by altered expression and activities in the pulmonary vasculature.[15-17] In fact, papaverine as a probe for PAH in a previous report,[11] could inhibit PDE10A, PDE3A, and PDE4A with IC_{50} values of 40 nM, 287 nM, and 1.6 μM,[9,5,17] respectively, potentially resulting in a false-positive action of PDE10A in PAH[11] due to contributions from other PDE subtypes (PDE3A and PDE4A). The treatment effect of papaverine on pulmonary hypertensive hemodynamic parameters in MCT-PAH rats may be related to the multiple inhibition of PDEs subfamilies such as PDE10, PDE3, and PDE4. The similar phenomenon occurs with sildenafil, a PDE5 inhibitor, whose therapeutic effect might be linked to some extent to its inhibition on PDE1C.[15] In order to exclude disturbance from other PDE subtypes, highly selective PDE10A inhibitors are generally valuable to further validate the feasibility of PDE10A as a novel target of PAH.

Herein, we combined the molecular dynamics (MD)-based design/optimization protocol with an integrated strategy (cocrystal structure, structural optimization, bioassay, and pharmacodynamic evaluation), which dramatically accelerated the hit-to-lead process and minimized the need for

chemical synthesis, to identify a highly selective PDE10 inhibitor **2b** (IC_{50} of 0.44 nM towards PDE10 and selectivity of over 45 000-fold against other PDEs). Compound **2b** significantly decreased the arterial pressure in PAH rats at a dosage of 2.5 mg/kg, thus validated PDE10 as a potential drug target for PAH.

■ RESULTS AND DISCUSSION

MD-based virtual screening (Figure 1) remarkably accelerated the discovery of PDE10A inhibitors with novel scaffolds. The commercially available database SPECS (http://www.specs.net), which consists of approximately 200 000 compounds, was selected for virtual screening and all compounds were filtered by Lipinski's Rule of Five[19] to improve the pharmacological properties of screened compounds.

A 3D-pharmacophore model was generated from the X-ray crystal structures of PDE10A in complex with a variety of ligands (PDB ID: 3QPN, 3QPO, 3QPP, 5DH4, and 5DH5).[4,20] In the established model, pharmacophore features and structural motifs included aromatic rings, hydrophobic side chains, and H-bond donor and acceptor groups in ligands. Moreover, the volume of the amino acid residues was added as an exclusion feature. A test set containing 193 active compounds selected from the Binding Database (http://www.bindingdb.org) and 9187 inactive compounds randomly generated from the DUD-E database (http://dude.docking.org/), was prepared for the goodness of hit (GH) test. The GH test score was 0.56, indicating that the model effectively picked out active PDE10A inhibitors (see Table S1 in the Supporting Information). Furthermore, a PAINS (pan-assay interfering compound substructures) screen was applied to remove possible false positive compounds using the online program PAINS-Remover.[21] Afterwards, 1091 molecules were retained.

Insert Figure 1 here.

All the molecules that passed the pharmacophore model and PAINS screening were docked into the PDE10A catalytic pocket to predict their binding patterns and the docking results were preliminarily selected by docking scores. More importantly, most potent and selective PDE10A inhibitors were reported to interact with the unique PDE10A selectivity pocket, which was first identified in the cocrystal structure of the clinical candidate **PF-2545920** with PDE10A.[22] In addition to the conserved interactions with residues Gln726 and Phe729, **PF-2545920** formed an H-bond with Tyr693 in the selectivity pocket, which was important to maintain potency and selectivity (Figure S1 in supporting information). Based on the evidence, only diverse hits that potentially interacted with selectivity pocket were pursued in our docking screen, and 47 molecules were retained.

MD simulations were also performed to precisely predict binding patterns and binding free

energies were estimated *via* the molecular mechanics/Poisson-Boltzmann surface area (MM/PBSA) and the molecular mechanics/Generalized Born surface area (MM/GBSA) methods.[23,24] Finally, only 23 compounds with stable MD simulation trajectories and considerable binding free energies were purchased and evaluated by bioassay.

Encouragingly, 13 of the selected 23 compounds exhibited greater than 50% inhibition at 10 μM (see Table S2 and Figure S2 in the Supporting Information). The hit ratio was up to 57% and eight novel scaffolds were discovered (Figure S2). Notably, compounds **AF-399/41980954** and **AF-399/14387019** showed considerable potency with IC_{50} values of 39 and 68 nM, respectively (Figure 1). In comparison with the inhibitory profiles of high throughput screening (HTS) reported in previous studies,[22,25,26] our hits had comparable or even better potency towards PDE10A, thus confirming the efficiency of the MD-based virtual screening.

The cocrystal structure of PDE10A in complex with AF-399/14387019 revealed binding mode consistent with the predicted one. Among the 13 active compounds identified, compound **AF-399/41980954** exhibited the strongest inhibition, but its imidazo[1,2-*a*]pyrimidine scaffold and isomers were already reported in other PDE10 inhibitors.[27-30] As we aimed to identify PDE10A inhibitors with novel scaffolds, **AF-399/14387019** was selected for further structural optimization.

The cocrystal structure of PDE10A with hit **AF-399/14387019** was determined (PDB ID: 6IJH) and the electron density in (2Fo–Fc) and (Fo–Fc) unambiguously showed that **AF-399/14387019** bound to the catalytic pocket of PDE10A (Figure 2A). The 1,8-naphthalimide group of **AF-399/14387019** was sandwiched by the hydrophobic residues Phe729 on one side and Phe696/Ile692 on the other side, and the carbonyl oxygen formed an H-bond with the amide nitrogen of Gln726. The H-bond with Gln726 and stacking against Phe729 are two characteristic binding modes conserved in other PDE inhibitors. Additionally, the ethyl linker of **AF-399/14387019** stretched towards the selectivity pocket, which was partially occupied by the coupled 1, 2, 4-triazole ring. An H-bond between the nitrogen of triazole ring and phenolic hydroxyl group of Tyr693 was also observed. Notably, the binding mode observed in the crystal structure superimposed well with the predicted pattern derived from the MD simulation (Figure 2B), confirming the reliability of the MD-based virtual screening protocol employed in the present study.

MD simulations greatly facilitated the 1st-round optimization. Currently, research on PDE10A inhibitors usually begins with HTS to identify novel scaffolds,[22,25-27,31-35] and a selective pocket binding group (SPBG) is then integrated into the scaffold by a linker to promote the interaction with Tyr693 (see Figure S1 in supporting information).[4,34-39] As the selectivity pocket maintains a relatively

defined shape, only groups with an appropriate volume fit well. However, a universal SPBG for PDE10A inhibitors has not been determined. As the result, a large number of analogues must be synthesized to identify a suitable SPBG, which is very time-consuming and costly.

Insert Figure 2 here.

Based on the cocrystal structure of PDE10A in complex with **AF-399/14387019**, *in silico* docking and MD simulations were used to identify the suitable SPBG for synthesis. As described above, the 1,8-naphthalimide group of **AF-399/14387019** functioned as the scaffold to interact with the conserved Gln726 and the hydrophobic clamp of PDE10A, while the coupled 1, 2, 4-triazole ring partially occupied the selectivity pocket. In the subsequent modification procedures, different combinations of linkers and heterocyclic SPBG were designed and subjected to *in silico* docking and MD simulations (Figure 3). According to the MM/PBSA binding free energies, the top five compounds (**1a** and **1c-1f**) were selected and synthesized (Table 1). Quinoline, a common scaffold of current PDE10A inhibitors, well fits the selectivity pocket and was attached to the 1, 8-naphthalimide core *via* an ethyl linker to form compound **1a**. Compound **1c** was designed with an ethyl linker and 4-phenyl-imidazole scaffold as the binding group while **1d** used 5-methyl-benzimidazole as the binding group. Compounds **1e** and **1f** contained longer linkers and a benzimidazole scaffold and were designed based on another hit **AR-422/43115142**. On the other hand, compound **1b** with a pyridine ring was designed as a negative reference and predicted to be less potent in comparison with **AF-399/14387019** (-25.7 vs -28.7 kcal/mol of MM/PBSA binding free energies).

Insert Figure 3 here.

Insert Table 1 here.

Insert Scheme 1 here.

Insert Scheme 2 here.

Insert Scheme 3 here.

As expected, compounds **1a**, **1c**, and **1d** exhibited significant inhibitory potency against PDE10A with IC_{50} values ranging from 2.1 to 20 nM, which were better than hit **AF-399/14387019**. Moreover, the reference compound **1b** exhibited poor potency with an IC_{50} >1000 nM, showing that groups with a small volume were not suitable for the selectivity pocket. For compounds **1e** and **1f,** the low inhibitory affinities of them against PDE10A were not in accordance with the high predicated binding free energies. We speculated that configuration of the propyl linker in both compounds are too flexible to predict binding free energies precisely. Compared to compound **1d**, a heteroatom was added to the benzimidazole motifs in these two compounds, which might affect their inhibitory affinities.

The 2nd round of optimization resulted in subnanomolar PDE10A inhibitors. Inspired of the promising results from the 1st round, compound **1d** (IC_{50} of 2.1 nM) was selected as a new starting compound for the 2nd round design (Figure 3). Binding patterns from stable MD simulations illustrated that compound **1d** deeply occupied the selectivity pocket and formed an H-bond with Tyr693. However, some space in the selectivity pocket remained unoccupied. Comparing the inhibitory potencies of compounds **1a** and **1b**, we found that compounds with larger side chains displayed more potent binding affinities (Table 1). Thus, large substitution groups such as tetrahydropyran, phenyl and pyridyl rings were attached to the N-1 position of the 5-methyl-benzoimidazole scaffold. In addition, the 5-methyl-benzoimidazole scaffold of compound **1d** was replaced by 5-fluoro-benzoimidazole or 6-methyl-imidazopyridine.

Similarly, all designed compounds were subjected to *in silico* docking and MD simulations that showed the top five compounds (**2b-2f**) having binding free energies 5-8 kcal/mol lower than **1d** (Table 2). The binding modes from MD simulations predicted that all compounds adopted similar orientations to that in the PDE10A-**1d** complex, with some subtle differences. As the phenyl or pyridyl substituted 5-methyl-benzoimidazole in compounds **2b** and **2f** has a larger volume than **1d**, they were expected to properly occupy the selectivity pocket to enhance potency. However, the space for the tetrahydropyran group in **2a/2c** was relatively narrowed due to the location of residues Met713 and Ile711 near the selectivity pocket. We speculated that small planar rings may fit better in this space than larger aliphatic rings (Figure 2). The substituted groups on the benzoimidazole scaffold also affected the inhibitory activity. The inhibitory potency towards PDE10A will be decreased by perturbation of the electronic properties of the 1-phenyl-benzimidazole group from 5-methyl (**2c**) to 5-fluoro (**2a**), replacement of the 5-methyl-1-benzoimidazole group (**2b**) with 6-methyl-imidazopyridine (**2d**).

Insert Table 2 here.

Insert Scheme 4 here.

With the low binding free energies, compounds **2b**, **2e**, and **2f** showed improved PDE10 inhibition compared with compound **1d**, and had the IC_{50} values ranging from 0.44 to 1.0 nM. In particular, compound **2b** having the pyridyl group at the N-1 position of the 5-methyl-benzoimidazole scaffold displayed inhibitory potency of 0.44 nM, which equates to 4- and 154-fold increases in binding affinity compared with **1d** and **AF-399/14387019**, respectively. Notably, the inhibitory potency of lead compound **2b** was comparable to the PDE10A clinical candidates **TAK-063** and **PF-2545920** that have IC_{50} values of 0.3 nM and 0.37 nM, respectively.

Compound 2b shows high selectivity against other PDE isoforms.

In the two-round optimization, a series of compounds with different substituents on the side chain of hit **AF-399/14387019** were designed and 12 compounds with properly predicted binding free energies were synthesized. Among them, compound **2b** with the pyridyl group at the N-1 position of the 5-methyl-benzoimidazole scaffold exhibited highly potent inhibition of 0.44 nM towards PDE10A and > 20 μM against other PDEs (> 45 000-fold selectivity, Table 3), suggesting that it represents a suitable chemical probe to investigate the role of PDE10 in PAH with minimal interference from other PDEs. In general, the discovery of drug leads requires several rounds of design/optimization of linkers, substituent groups, and substantial amounts of synthetic work. In our approach, we took full advantage of binding free energy predictions to substantially accelerate the hit-to-lead process and minimize chemical loads of synthetic work.

Insert Table 3 here.

Insert Table 4 here.

Ligand profiling was performed to screen the binding affinities of compound **2b** at the Guangzhou Institutes of Biomedicine and Health against over twenty different targets in a panel of receptors, ion channels, and other enzyme*s*,[40-46] which would be beneficial to rule out other its non-target activities. The *in vitro* binding affinities of compound **2b** were shown in Table 4 and most of them (Estrogen receptor ER_α, Estrogen receptor ER_β, FGFR1, FGFR2, FGFR3, FGFR4, FLT3, ABL, Aurora A, Aurora B, PLK1, EGFR, ZAK, BRD4, COX2, HDAC1, HDAC6, AChE, and BChE) were > 10.0 μM except that against hERG potassium channel. The IC_{50} of **2b** towards hERG potassium channel was 4.7 μM, which was over 1000-fold higher than its inhibitory potency of 0.44 nM against PDE10A.

The cocrystal structure validated the predicted binding pattern of compound 2b with PDE10A. The cocrystal structure of PDE10A with lead **2b** was determined (PDB ID: 6IJI). As shown in Figure 4, the 1, 8-naphthalimide group of **2b** served as the scaffold to interact with the conserved residue Gln726 and hydrophobic clamp of PDE10A catalytic pocket. In comparison with hit **AF-399/14387019**, **2b** involves another H-bond interaction with Try693 in the selectivity pocket, which contributes to its high inhibitory potency against PDE10A and excellent selectivity over other PDEs. The binding pattern in the cocrystal structure of PDE10A-**2b** was superposed well with the predicted mode, validating that our modeling protocols were feasible and practical for design of PDE inhibitors, especially those with well-defined or special sub-pockets such as in the cases of PDE2, PDE4, and

PDE5.[47-49]

Insert Figure 4 here.

The pharmacokinetic profile assessment in SD rats after intravenous administration of 2.5 mg/kg **2b** was performed, and **2b** showed a C_{max} of 3500.87 ng/mL at T_{max} 0.083 h and AUC (0-t) of 1097.38 h*ng/mL in Table 5, respectively, indicating that it could give a reasonable blood exposure. In addition, its plasma protein binding (PPB) was 98%. On the basis of its pharmacokinetic profile, compound **2b** was further subjected to pharmacodynamics studies *in vivo*.

Insert Table 5 here.

The highly selective PDE10A inhibitor 2b significantly decreased the arterial pressure in PAH rats. The *in vivo* therapeutic effects of compound **2b** against PAH were measured. PAH was successfully induced in rats after 3 weeks of monocrotaline (MCT) injections, as shown by increase of the mean pulmonary artery pressure (mPAP), right ventricle hypertrophy index (RVHI%), and wall thickness percentage (WT%) of the model group in comparison with the control group (Figure 5A-5C). As a positive control, PDE5 inhibitor sildenafil at a dose of 10 mg/kg (p. o.) effectively ameliorated these medical indicators in the rats, further verifying the feasibility of our *in vivo* rat models. Under the same conditions, the values of mPAP (Figure 5A), RVHI% (Figure 5B), and WT% (Figure 5C) from the group treated with 2.5 mg/kg **2b** (i.p.) were significantly improved compared with the model group. Body weight results (Figure 5D) demonstrated the low toxicity of compound **2b**. In addition, PDE10 inhibitor **2b** could greatly increase the concentration of cAMP (Figure 5E) in lung and slightly increase the level of cGMP (Figure 5F) compared with the model group, demonstrating that the *in vivo* activity of compound **2b** was mediated by both cAMP and cGMP and the former played the major role. PDE5 inhibitor sildenafil remarkably improved the concentration of cGMP in lung, while the concentration of cAMP remained unchanged, suggested that the *in vivo* activity of sildenafil was predominantly mediated by cGMP rather than cAMP. Thus, our results suggested that lead compound **2b** is an effective anti-PAH agent.

PDE isoforms of PDE1, PDE2, PDE3, PDE4 PDE5, and PDE10 are expressed and regulated in the pulmonary vasculature of patients with PAH.[13] High selective inhibitors will be needed to identify which specific PDE is related to PAH. The cGMP-specific PDE5 is the most abundant isoform expressed in lung, and two PDE5 inhibitors (sildenafil and tadalafil) were approved as treatments for human PAH. Since compound **2b** shows high inhibitory potency against PDE10A (IC_{50} of 0.44 nM) and high selectivity over other PDEs (selectivity index > 45 000-fold), the anti-PAH effect of **2b** in rats would be achieved *via* selective inhibition on PDE10A rather than other PDEs, validating that PDE10 is a potential target for treatment of PAH.

Insert Figure 5 here.

Both PDE10A inhibitors 2b and PF-2545920 prevented HPASMC phenotypic transformation induced by platelet-derived growth factor. Vascular remodeling plays an important role in the development and complications of PAH. Vascular smooth muscle cells (VSMC) phenotypic transformation works as a major initiating factor for vascular remodeling in hypertension.[50] VSMC phenotypic transformation is characterized by an increase in synthetic protein including osteopontin (OPN) and proliferating cell nuclear antigen (PCNA), as well as a reduction in contractile proteins such as α-smooth muscle actin (α-SMA) and smooth muscle 22α (SM22α).[51] Thus, with the results obtained in the pharmacodynamic experiments, both PDE10A inhibitor **2b** and **PF-2545920** developed by Pfizer were applied in the platelet-derived growth factor (PDGF)-BB induced HPASMC model to assess the effects on VSMC phenotypic transformation. The results showed that both compound **2b** and **PF-2545920** reduced the level of OPN and PCNA (Figure S3A and S3B), and increased the level of α-SMA and SM22α (Figure S3C and S3D). Compound **PF-2545920** gave a better result on the regulation of OPN and SM22α, and gave a comparable result on the regulation of PCNA and α-SMA. These results indicated these two compounds modulate VSMC phenotypic transformation and further supported that PDE10 could work as a potential anti-PAH target.

■ CONCLUSION

In summary, an effective hit-to-lead strategy was introduced to identify a highly potent and selective PDE10A inhibitor **2b** (IC_{50} of 0.44 nM towards PDE10A and > 45 000-fold selectivity over other PDEs), which served as a probe to validate PDE10 as a potential anti-PAH target.

Remarkably, a hit ratio of 57% was achieved and 8 novel scaffolds were discovered by the MD-based virtual screening, confirming that the screening strategy was efficient and could serve as a complementary approach to the costly HTS method. By docking and MD simulations, the two-round optimization of hit **AF-399/14387019** were rapidly advanced and resulted in the discovery of compound **2b**. The cocrystal structures of PDE10A in complex with **AF-399/14387019** and **2b** revealed that their binding patterns were consistent with the predicted modes, verifying the MD-based design/optimization strategy used in the present study. Compound **2b** significantly decreased PAH in rats *in vivo*, and this improvement is probably achieved by selectively inhibiting PDE10A based on the high PDE selectivity of **2b**. These findings are consistent with PDE10A inhibition being a valid approach for treatment of PAH.

In short, our studies not only show that PDE10 inhibitors are potential therapeutics for treatment of PAH, but also open a new avenue to effectively discover highly selective PDE inhibitors *via* the integrated strategy.

■ EXPERIMENTAL SECTION

Chemistry. Unless specified, all reagents and starting materials were purchased from commercial sources and directly used as received. Analytical thin layer chromatography (TLC) was performed using pre-coated silica gel plate. Visualization was achieved by UV light (254 nm). Column chromatography was performed using silica gel. ^{1}H NMR and ^{13}C NMR spectra were recorded on a BrukerBioSpin GmbH spectrometer at 400.1 and 100.6 MHz, respectively. Coupling constants are given in Hz using TMS as an internal standard and $CDCl_3$ or DMSO-d_6 as solvents. Chemical shift is given in ppm (δ). High-resolution mass spectra (HRMS) were obtained on an IT-TOF mass spectrometer. The purity of compounds was determined by reverse-phase high-performance liquid chromatography (HPLC) and confirmed to be more than 95%. HPLC instrument: SHIMADZU LC-20AT (column, Hypersil BDS C18, 5.0 μm, 4.6 mm×150 mm (Elite); detector, SPD-20A UV/vis detector, UV detection at 254 nm; elution, MeOH in water (60%, v/v); T = 25°C; flow rate = 1.0 mL/min).

General procedures for synthesis of compounds 1a-1b. A suspension of 1,8-naphthalic anhydride **7** (198 mg, 1.0 mmol) and appropriate aliphatic amine (2.0 mmol) in ethanol (10 mL) was heated under reflux for 3 h. After evaporation of solvent under reduced pressure, the crude product was purified on a silica gel column with chloroform/methanol (100:1) to give compounds **1a-1b** as a colorless solid.

2-(2-(quinolin-2-yl)ethyl)-1H-benzo[de]isoquinoline-1,3(2H)-dione (1a). Colorless solid. Yield: 85%; purity: 96.6%; Mp: 199.7-210.3 °C; ^{1}H NMR (400 MHz, $CDCl_3$) δ 8.61 (dd, J = 7.3, 1.1 Hz, 2H), 8.24 (dd, J = 8.3, 1.0 Hz, 2H), 8.10 (d, J = 8.4 Hz, 1H), 7.98 (d, J = 8.4 Hz, 1H), 7.78 (dt, J = 8.2, 5.7 Hz, 3H), 7.68 – 7.63 (m, 1H), 7.53 – 7.45 (m, 2H), 4.77 – 4.71 (m, 2H), 3.45 (dd, J = 8.4, 6.9 Hz, 2H); ^{13}C NMR (101 MHz, $CDCl_3$) δ 164.1×2, 159.4, 148.0, 136.2, 133.8×2, 131.6, 131.2×2, 129.2, 129.1, 128.2, 127.4, 126.9×2, 126.9, 125.8, 122.8, 121.6×2, 39.9, 37.1; HRMS (ESI-TOF) m/z calcd for $C_{23}H_{16}N_2O_2$ $[M+H]^+$ 353.1285, found 353.1275.

2-(2-(pyridin-2-yl)ethyl)-1H-benzo[de]isoquinoline-1,3(2H)-dione (1b). Colorless solid. Yield: 83%; purity: 99.9%; Mp: 143.7-145.4 °C; ^{1}H NMR (400 MHz, $CDCl_3$) δ 8.59 (d, J = 7.2 Hz, 2H), 8.54 (d, J = 4.2 Hz, 1H), 8.21 (d, J = 8.1 Hz, 2H), 7.75 (t, J = 7.7 Hz, 2H), 7.59 (td, J = 7.7, 1.6 Hz, 1H), 7.26 (d, J = 6.9 Hz, 1H), 7.12 (dd, J = 6.9, 5.3 Hz, 1H), 4.64 – 4.55 (m, 2H), 3.28 – 3.18 (m, 2H); ^{13}C NMR (101 MHz, $CDCl_3$) δ 164.0×2, 159.0, 149.4, 136.3, 133.9×2, 131.6, 131.2×2, 128.2, 126.9×2, 123.3×2, 122.7, 121.5, 40.1, 36.4; HRMS (ESI-TOF) m/z calcd for $C_{19}H_{14}N_2O_2$ $[M+H]^+$ 303.1128, found 303.1122.

General procedures for synthesis of compounds 1c-1d. To a mixture of appropriate amine (1.0

mmol) in dichloromethane (5 mL) was added HATU (570 mg, 1.5 mmol), *N*, *N*-diisopropylethylamine (516 mg, 4.0 mmol) and **9** (269 mg, 1.0 mmol), and stirred at room temperature for 12 h. The mixture was diluted with saturated sodium bicarbonate aqueous solution and extracted with dichloromethane (300 mL). The organic layer was washed with brine, dried over anhydrous sodium sulfate, filtered and concentrated *in vacuo* to get a residue. To a solution of this residue in acetic acid glacial (5 mL) was added ammonium acetate (1.38 g, 18.0 mmol). The resulting mixture was heated at reflux for 7 h. After being cooled to room temperature, brine was added and the mixture was separated. The aqueous phase was extracted with ethyl acetate (300 mL), the organic phase was dried over sodium sulfate. After filtration and concentration, the residue was purified by column chromatography on silica gel (petroleum/ethyl acetate, 1:1) to yield compounds **1c-1d**.[52]

2-(2-(4-phenyl-1H-imidazol-2-yl)ethyl)-1H-benzo[de]isoquinoline-1,3(2H)-dione (1c). Colorless solid. Yield: 63%; purity: 99.9 %; Mp: 132.5-136.3 °C; ^{1}H NMR (400 MHz, DMSO – d_6) δ 8.47 (dd, J = 9.9, 7.8 Hz, 4H), 7.90 – 7.83 (m, 2H), 7.65 – 7.58 (m, 2H), 7.42 (s, 1H), 7.28 (t, J = 7.6 Hz, 2H), 7.14 (t, J = 7.3 Hz, 1H), 4.47 – 4.36 (m, 2H), 3.04 (t, J = 7.5 Hz, 2H); ^{13}C NMR (101 MHz, DMSO – d_6) δ 163.9×2, 146.0, 134.7×2, 131.8, 131.1×3, 128.8×2, 127.9, 127.6×3, 126.3, 124.5×3, 122.7×2, 39.1, 26.8; HRMS (ESI-TOF) m/z calcd for $C_{23}H_{17}N_3O_2$ $[M+H]^+$ 368.1394, found 368.1384.

2-(2-(5-methyl-1H-benzo[d]imidazol-2-yl)ethyl)-1H-benzo[de]isoquinoline-1,3(2H)-dione (1d). Colorless solid. Yield: 54%; purity: 96.7%; Mp: 138.0-142.0 °C; ^{1}H NMR (400 MHz, MeOD) δ 8.52 (dd, J = 7.3, 1.0 Hz, 2H), 8.39 – 8.34 (m, 2H), 7.84 – 7.78 (m, 2H), 7.32 (d, J = 8.2 Hz, 1H), 7.25 (s, 1H), 7.01 (d, J = 8.4 Hz, 1H), 4.63 (t, J = 7.1 Hz, 2H), 3.30 (d, J = 7.1 Hz, 2H), 2.43 (s, 3H); ^{13}C NMR (101 MHz, DMSO– d_6) δ 163.8×2, 152.2, 134.8×2, 134.7, 131.8, 131.1×2, 131.0, 128.0, 127.6×2, 127.5, 123.3×2, 122.6, 114.9, 114.3, 38.7, 27.5, 21.7; HRMS (ESI-TOF) m/z calcd for $C_{22}H_{17}N_3O_2$ $[M+H]^+$ 356.1394, found 356.1385.

General procedures for synthesis of compounds 1e-1f. Sodium hydride (48 mg, 1.2 mmol) was added to a solution of benzimidazole (1.0 mol) in DMF (5 mL) at 0 °C. The mixture stirred at 0 °C for 15 min, and **11** (317 mg, 1.0 mmol) was added at 0 °C. The reaction was stirred at room temperature for 2 h, quenched with MeOH and then concentrated to dryness. The resulting crude was purified by silica gel column chromatography (CH_2Cl_2) to afford compounds **1e-1f** as a colorless solid.

2-(3-((1H-benzo[d]imidazol-2-yl)amino)propyl)-1H-benzo[de]isoquinoline-1,3(2H)-dione (1e) . Colorless solid. Yield: 84%;purity: 95.6%; Mp: 197.9-200.5 °C; ^{1}H NMR (400 MHz, $CDCl_3$) δ 8.60 (d, J = 7.3 Hz, 2H), 8.23 (d, J = 8.2 Hz, 2H), 7.76 (td, J = 8.2, 2.0 Hz, 2H), 7.39 (d, J = 7.2 Hz, 1H), 7.15 – 7.01 (m, 3H), 4.28 (dd, J = 8.8, 4.0 Hz, 2H), 4.09 (t, J = 7.0 Hz, 2H), 2.34 – 2.27 (m, 2H); ^{13}C NMR (101 MHz, $CDCl_3$) δ 164.6×2, 147.6, 141.6, 134.4×2, 133.9, 131.6×2, 131.5, 128.2, 127.1×2, 122.3×2, 121.7, 119.9, 116.3, 107.8, 88.3, 80.6, 78.9, 50.5, 41.2, 37.9, 28.3;HRMS (ESI-TOF) m/z

calcd for $C_{22}H_{18}N_4O_2$ $[M+H]^+$ 371.1503, found 371.1500.

2-(3-((1H-benzo[d]imidazol-2-yl)thio)propyl)-1H-benzo[de]isoquinoline-1,3(2H)-dione(1f). Colorless solid .Yield: 75%; purity: 95.7%; Mp: 177.3-178.2 °C; ^{1}H NMR (400 MHz, $CDCl_3$) δ 10.04 (s, 1H), 8.65 (d, J = 7.3 Hz, 2H), 8.26 (d, J = 8.2 Hz, 2H), 7.80 (t, J = 7.7 Hz, 2H), 7.69 – 7.61 (m, 1H), 7.43 (d, J = 5.0 Hz, 1H), 7.25 – 7.19 (m, 2H), 4.54 – 4.46 (m, 2H), 3.36 (t, J = 6.6 Hz, 2H), 2.18 (dd, J = 14.0, 7.0 Hz, 2H); ^{13}C NMR (101 MHz, $CDCl_3$) δ 164.4×2, 148.8, 144.1, 134.9, 134.2×2, 131.6, 131.4×2, 128.2, 127.0×2, 122.7, 122.5×2, 122.0, 118.7, 110.2, 39.0, 31.3, 30.0; HRMS (ESI-TOF) m/z calcd for $C_{22}H_{17}N_3O_2S$ $[M+H]^+$ 388.1114, found 388.1115.

General procedures for synthesis of compounds 2a-2f. To a mixture of appropriate amine (1.0 mmol) in CH_2Cl_2 (15 mL) were added HATU (380 mg, 1.5 mmol), *N*, *N*-diisopropylethylamine (516 mg, 4.0 mmol) and **9** (322 mg, 1.2 mmol), and stirred at room temperature for 12 h. The mixture was diluted with saturated sodium bicarbonate aqueous solution (100 mL) and extracted with dichloromethane (300 mL). The organic layer was washed with brine, dried over anhydrous sodium sulfate, filtered and concentrated in vacuo. To the residue was added AcOH (20 mL), and stirred at 90 °C for 12 h. Then the reaction mixture was concentrated in vacuo. The residue was diluted with saturated sodium bicarbonate aqueous solution and extracted with dichloromethane. The organic layer was washed with brine, dried over anhydrous sodium sulfate, filtered and concentrated in vacuo. The residue was purified by silica gel column chromatography (petroeum/ethyl acetate, 10:1) to give compounds **2a-2f** as a colorless solid.

2-(2-(5-fluoro-1-(tetrahydro-2H-pyran-4-yl)-1H-benzo[d]imidazol-2-yl)ethyl)-1H-benzo[de]isoquinoline-1,3(2H)-dione (2a). Colorless solid. Yield: 72%; purity: 98.9%; Mp: 236.6-237.9 °C; ^{1}H NMR (400 MHz, $CDCl_3$) δ 8.62 (dd, J = 7.3, 1.0 Hz, 2H), 8.25 (dd, J = 8.3, 0.9 Hz, 2H), 7.78 (dd, J = 8.1, 7.4 Hz, 2H), 7.54 (dd, J = 8.9, 4.5 Hz, 1H), 7.39 (dd, J = 9.3, 2.5 Hz, 1H), 7.04 – 6.96 (m, 1H), 4.84 (ddd, J = 12.2, 7.9, 4.5 Hz, 1H), 4.65 – 4.59 (m, 2H), 4.22 (dd, J = 11.7, 4.4 Hz, 2H), 3.73 (dd, J = 11.9, 10.5 Hz, 2H), 3.41 – 3.35 (m, 2H), 2.66 (dd, J = 12.8, 4.6 Hz, 2H), 1.96 (dd, J = 12.8, 2.7 Hz, 2H); ^{13}C NMR (101MHz, $CDCl_3$) δ 164.0×2, 160.2, 157.8, 152.7, 134.2×2, 131.7, 131.4×2, 130.0, 128.2, 127.0×2, 122.5×2, 112.0 (d, J = 10.0 Hz), 110.3 (d, J = 25.9 Hz), 105.5 (d, J = 23.8 Hz), 67.5×2, 53.2, 38.5, 31.4×2, 26.95; HRMS (ESI-TOF) m/z calcd for $C_{26}H_{22}N_3O_3F$ $[M+H]^+$ 444.1718, found 444.1706.

2-(2-(5-methyl-1-(pyridin-4-yl)-1H-benzo[d]imidazol-2-yl)ethyl)-1H-benzo[de]isoquinoline -1,3(2H) -dione (2b). Colorless solid. Yield: 78%; purity: 99.7 %; Mp: 200.6-206.6 °C; ^{1}H NMR (400 MHz, $CDCl_3$) δ 8.75 (dd, J = 4.5, 1.6 Hz, 2H), 8.54 (dd, J = 7.3, 1.0 Hz, 2H), 8.23 (dd, J = 8.3, 1.0 Hz, 2H), 7.75 (dd, J = 8.1, 7.4 Hz, 2H), 7.53 (s, 1H), 7.44 (dd, J = 4.5, 1.6 Hz, 2H), 7.10 (dd, J =

2.7, 0.9 Hz, 2H), 4.69 (t, *J* = 7.4 Hz, 2H), 3.32 (t, *J* = 7.4 Hz, 2H), 2.49 (s, 3H); ^{13}C NMR (101 MHz, $CDCl_3$) δ 164.0×2, 151.8×2, 151.1, 148.8, 143.7, 143.3, 134.1×2, 133.3, 132.8, 131.6, 131.3×2, 126.9×2, 124.8, 122.5, 121.4×2, 119.6×2, 109.3, 38.3, 26.4, 21.5; HRMS (ESI-TOF) m/z calcd for $C_{27}H_{20}N_4O_2$ $[M+H]^+$ 433.1659, found 433.1656.

2-(2-(5-methyl-1-(tetrahydro-2H-pyran-4-yl)-1H-benzo[d]imidazol-2-yl)ethyl)-1H-benzo [de]isoquinoline-1,3(2H)-dione (2c). Colorless solid. Yield: 68%; purity: 95.0%; Mp: 200.3-204.1 °C; ^{1}H NMR (400 MHz, $CDCl_3$) δ 8.64 (d, *J* = 7.2 Hz, 2H), 8.25 (d, *J* = 8.1 Hz, 2H), 7.79 (t, *J* = 7.8 Hz, 2H), 7.51 (d, *J* = 8.8 Hz, 2H), 7.07 (d, *J* = 8.3 Hz, 1H), 4.83 (t, *J* = 4.3 Hz, 1H), 4.63 (dd, *J* = 9.1, 6.9 Hz, 2H), 4.22 (dd, *J* = 11.7, 4.4 Hz, 2H), 3.73 (t, *J* = 11.2 Hz, 2H), 3.40 – 3.33 (m, 2H), 2.70 (qd, *J* = 12.6, 4.7 Hz, 2H), 2.48 (s, 3H), 1.94 (dd, *J* = 12.8, 2.7 Hz, 2H); ^{13}C NMR (101 MHz, $CDCl_3$) δ 164.0×2, 151.1, 143.7, 134.1×2, 131.7, 131.6, 131.4×2, 131.3, 128.2, 126.9×2, 123.5×2, 122.5, 119.7, 111.2, 67.6×2, 53.0, 38.7, 31.5×2, 27.0, 21.3; HRMS (ESI-TOF) m/z calcd for $C_{27}H_{25}N_3O_3$ $[M+H]^+$ 440.1969, found 440.1956.

2-(2-(6-methyl-3-(pyridin-4-yl)-3H-imidazo[4,5-b]pyridin-2-yl)ethyl)-1H-benzo[de] isoquinoline-1,3(2H)-dione (2d). Colorless solid. Yield: 74%; purity: 98.3%; Mp: 223.3-223.8 °C; ^{1}H NMR (400 MHz, $CDCl_3$) δ 8.73 (dd, *J* = 4.6, 1.6 Hz, 2H), 8.54 (dd, *J* = 7.3, 1.0 Hz, 2H), 8.24 (dd, *J* = 8.3, 0.9 Hz, 2H), 8.18 (d, *J* = 1.6 Hz, 1H), 7.81 (d, *J* = 1.0 Hz, 1H), 7.76 (dd, *J* = 8.0, 7.5 Hz, 2H), 7.50 (dd, *J* = 4.6, 1.6 Hz, 2H), 4.70 (t, *J* = 7.2 Hz, 2H), 3.39 (t, *J* = 7.3 Hz, 2H), 2.49 (s, 3H); ^{13}C NMR (101 MHz, $CDCl_3$) δ 164.0×2, 152.6, 151.4×2, 146.7, 145.0, 142.1, 135.0, 134.1×2, 131.6, 131.4×2, 128.9, 128.2, 127.4, 127.0×2, 122.4×2, 121.7×2, 38.1, 27.0, 18.6; HRMS (ESI-TOF) m/z calcd for $C_{28}H_{21}N_5O_2$ $[M+H]^+$ 434.1612, found 434.1609.

2-(2-(6-methyl-3-phenyl-3H-imidazo[4,5-b]pyridin-2-yl)ethyl)-1H-benzo[de]isoquinoline-1,3(2H)-dione (2e). Colorless solid. Yield: 54%; purity: 99.9%; Mp: 230.2-231.1 °C; ^{1}H NMR (400 MHz, $CDCl_3$) δ 8.52 (dd, *J* = 7.3, 1.0 Hz, 2H), 8.22 (dd, *J* = 8.3, 0.9 Hz, 2H), 8.16 (d, *J* = 1.5 Hz, 1H), 7.79 – 7.71 (m, 3H), 7.46 (d, *J* = 3.9 Hz, 4H), 7.42 – 7.38 (m, 1H), 4.69 (t, *J* = 7.2 Hz, 2H), 3.30 (t, *J* = 7.2 Hz, 2H), 2.47 (s, 3H); ^{13}C NMR (101 MHz, $CDCl_3$) δ 163.9×2, 153.6, 147.6, 144.7, 134.8, 134.5, 133.9×2, 131.6, 131.2×2, 129.7×2, 128.8, 128.3, 128.0, 127.6×2, 126.9, 126.8×2, 122.6×2, 38.2, 26.8, 18.6; HRMS (ESI-TOF) m/z calcd for $C_{27}H_{20}N_4O_2$ $[M+H]^+$ 433.1659, found 433.1651.

2-(2-(5-methyl-1-phenyl-1H-benzo[d]imidazol-2-yl)ethyl)-1H-benzo[de]isoquinoline-1,3 (2H)-dione (2f). Colorless solid. Yield: 88%; purity: 97.7%; Mp: 208.8-211.9 °C; ^{1}H NMR (400 MHz, $CDCl_3$) δ 8.52 (d, *J* = 7.2 Hz, 2H), 8.20 (d, *J* = 8.2 Hz, 2H), 7.73 (t, *J* = 7.7 Hz, 2H), 7.52 – 7.38 (m, 6H), 7.01 (t, *J* = 6.3 Hz, 2H), 4.69 (t, *J* = 7.3 Hz, 2H), 3.25 (t, *J* = 7.3 Hz, 2H), 2.48 (s, 3H); ^{13}C NMR (101 MHz, $CDCl_3$) δ 163.9×2, 152.0, 143.0, 136.0, 134.7, 133.9×2, 131.9, 131.6, 131.2×2, 129.8×2,

128.6, 128.2, 127.3×2, 126.8×2, 124.1×2, 122.6, 119.1, 109.5, 38.4, 26.3, 21.5; HRMS (ESI-TOF) m/z calcd for $C_{28}H_{21}N_3O_2$ $[M+H]^+$ 432.1707, found 432.1703.

General procedures for synthesis of compounds 4a-4b. To a solution of 2-(quinolin-2-yl)ethanol (**3a**) or 2-(pyridin-2-yl)ethanol(**3b**) (2.0 mmol) in distilled dichloromethane (10 mL) was added thionyl chloride (5.2 mmol) under a calcium chloride tube. The solution was stirred at room temperature for 1 h. After concentration under reduced pressure, the mixture was diluted with ethyl acetate (350 mL) and washed with brine (20 mL). The organic layer was dried over anhydrous sodium sulfate, filtered and concentrated under reduced pressure to give compounds **4a-4b** as yellow powder.[53]

2-(2-chloroethyl)quinoline (4a). Yellow powder. Yield: 94%; ^{1}H NMR (400 MHz, $CDCl_3$) δ 8.98 (d, J = 8.2 Hz, 1H), 8.82 (s, 1H), 8.13 (d, J = 7.4 Hz, 1H), 8.08 – 8.02 (m, 1H), 7.87 (s, 2H), 4.23 (s, 2H), 3.99 (s, 2H).

2-(2-chloroethyl)pyridine (4b). Yellow powder. Yield: 65%; ^{1}H NMR (400 MHz, $CDCl_3$) δ 8.52 (s, 1H), 7.59 (t, J = 6.7 Hz, 1H), 7.23 – 7.06 (m, 2H), 3.89 (dt, J = 5.9, 2.7 Hz, 2H), 3.20 (t, J = 6.2 Hz, 2H).

General procedures for synthesis of compounds 5a-5b. To the solution of 2-(2-chloroethyl)quinoline or 2-(2-chloroethyl)pyridine (5.0 mmol) in DMF (30 mL) was added sodium azide (975 mg, 15.0 mmol). The mixture was warmed to 70 ^{o}C and stirred for 12 h. After the solution was cooled to room temperature, water was added. The solution was extracted with ethyl acetate (300 mL) and washed with water and brine. The organic solution was dried over anhydrous sodium sulfate, concentrated in vacuo. The residue was purified by silica gel chromatography (petroleum/ethyl acetate, 10:1) to afford compounds **5a-5b** as a colorless solid.[54]

2-(2-azidoethyl)quinoline (5a). Colorless solid. Yield: 86%; ^{1}H NMR (400 MHz, $CDCl_3$) δ 8.10 (dd, J = 18.1, 8.4 Hz, 2H), 7.83 (t, J = 10.2 Hz, 1H), 7.73 (ddd, J = 8.4, 7.0, 1.4 Hz, 1H), 7.57 – 7.50 (m, 1H), 7.35 (t, J = 10.0 Hz, 1H), 3.91 – 3.81 (m, 2H), 3.31 – 3.22 (m, 2H).

2-(2-azidoethyl)pyridine (5b). Colorless solid. Yield: 79%; ^{1}H NMR (400 MHz, $CDCl_3$) δ 8.61 – 8.55 (m, 1H), 7.64 (td, J = 7.7, 1.8 Hz, 1H), 7.25 – 7.14 (m, 2H), 3.77 – 3.70 (m, 2H), 3.08 (q, J = 6.6 Hz, 2H).

General procedures for synthesis of compounds 6a-6b. To a solution of **5a-5b** (5.0 mmol)in 1,4-dioxane /ethanol (30 mL, 1:1, v:v) was added Pd/C (100 mg, 10%). After a 4 h agitation at room temperature with H_2, the mixture was filtered and washed with ethanol. The filtrate was evaporated, recrystallized from ethanol to give compounds **6a-6b** as a brown oil.

2-(quinolin-2-yl)ethanamine (6a). Brown oil. Yield: 92%; ^{1}H NMR (400 MHz, $CDCl_3$) δ 8.06 (dd, J = 14.9, 8.5 Hz, 2H), 7.78 (d, J = 8.1 Hz, 1H), 7.69 (t, J = 7.6 Hz, 1H), 7.50 (t, J = 7.5 Hz, 1H),

7.31 (d, J = 8.4 Hz, 1H), 3.23 (t, J = 6.5 Hz, 2H), 3.13 (t, J = 6.5 Hz, 2H).

2-(pyridin-2-yl)ethanamine (6b). Colorless solid. Yield: 91%; ^{1}H NMR (400 MHz, $CDCl_3$) δ 8.52 (d, J = 4.2 Hz, 1H), 7.58 (tt, J = 6.6, 3.3 Hz, 1H), 7.19 – 7.08 (m, 2H), 3.07 (d, J = 24.3 Hz, 2H), 2.91 (t, J = 6.7 Hz, 2H).

Methyl 3-(1,3-dioxo-1H-benzo[de]isoquinolin-2(3H)-yl)propanoate (8). To a solution of 1H-benzo[de]isoquinoline-1,3(2H)-dione **7** (197 mg, 1.0 mmol) in DMF (30 mL) was added cesium carbonate (553 mg, 4.0 mmol) and methyl 3-bromopropanoate (495 mg, 3.0 mmol), and the mixture was refluxed for 12 h at 120 ^{o}C. After completion of the reaction, the solid was removed by filtration and then poured into water and extracted with ethyl acetate (300 mL), the solvent was evaporated under reduced pressure to get the crude product. This residue was further purified by silical gel column chromatography (petroleum/ethyl acetate, 10:1) to afford compound **8** (249 mg).[55] Yield: 88%; ^{1}H NMR (400 MHz, $CDCl_3$) δ 8.60 (d, J = 7.3 Hz, 2H), 8.22 (d, J = 8.2 Hz, 2H), 7.76 (t, J = 7.8 Hz, 2H), 4.51 (t, J = 7.5 Hz, 2H), 3.70 (s, 3H), 2.78 (t, J = 7.5 Hz, 2H).

3-(1,3-dioxo-1H-benzo[de]isoquinolin-2(3H)-yl)propanoic acid (9). Compound **8** (2.83 g, 10.0 mmol) was treated with 1N aqueous sodium hydroxide (22 mL, 22.0 mmol) in EtOH (40 mL), and stirred overnight at room temperature. Additional 1N aqueous sodium hydroxide (22 mL, 22.0 mmol) was added, and the reaction was stirred for 6 h at room temperature. The mixture was acidified with 1N aqueous HCl to pH = 3-4 and extracted with ethyl acetate (300 mL) and washed with water and brine. The organic solution was dried and concentrated to give compound **9** as a colorless solid (2.09 g).[56] Yield: 78%; ^{1}H NMR (400 MHz, DMSO – d_6) δ 12.33 (s, 1H), 8.47 (dd, J = 13.5, 7.3 Hz, 4H), 7.87 (t, J = 7.1 Hz, 2H), 4.27 (t, J = 7.4 Hz, 2H), 2.61 (t, J = 7.5 Hz, 2H).

2-(3-bromopropyl)-1H-benzo[de]isoquinoline-1,3(2H)-dione (10). To a solution of 1,8-naphthalimide **7** (197 mg, 1.0 mmol) in acetonitrile (30 mL), anhydrous potassium carbonate (553 mg, 4.0 mmol) and 1,3-dibromopropane (597 mg, 3.0 mmol) were added and the mixture was refluxed for 12 h. After completion of the reaction, potassium carbonate was removed by filtration and the solvent was evaporated under reduced pressure to get the crude product. This was further purified by silica gel column chromatography (petroleum/ethyl acetate, 10:1) to afford compound **10** (285 mg).[57,58] Yield: 90%; ^{1}H NMR (400 MHz, $CDCl_3$) δ 8.63 (dd, J = 14.3, 7.3 Hz, 2H), 8.25 (t, J = 11.3 Hz, 2H), 7.79 (dt, J = 15.5, 7.6 Hz, 2H), 4.37 (dt, J = 14.1, 7.1 Hz, 2H), 3.54 (dt, J = 13.8, 6.9 Hz, 2H), 2.42 – 2.31 (m, 2H).

General procedures for synthesis of compounds 12a-12b. To a solution of nitrobenzene **11a-11b** (1.0 mmol) in dioxne (5.0 mL) was added appropriate aniline (1.1 mmol). The solution was then refluxed for 4 hours and allowed to cool to room temperature and was diluted with ethyl acetate (75 mL). The organic layer was washed with water (75 mL), brine (75 mL), and dried over anhydrous

sodium sulfate. After concentration *in vacuo* the residue was purified by silica gel column chromatography (petroleum/ethyl acetate, 10:1) to get products **12a-12b** as orange oil.

N-(4-fluoro-2-nitrophenyl)tetrahydro-2H-pyran-4-amine (12a). Orange oil. Yield: 52%; ^{1}H NMR (400 MHz, $CDCl_3$) δ 7.99 (d, J = 5.9 Hz, 1H), 7.92 (dd, J = 9.2, 3.0 Hz, 1H), 7.29 – 7.23 (m, 1H), 6.88 (dd, J = 9.5, 4.5 Hz, 1H), 4.04 (dt, J = 12.0, 3.9 Hz, 2H), 3.78 – 3.68 (m, 1H), 3.64 – 3.54 (m, 2H), 2.13 – 2.04 (m, 2H), 1.75 – 1.65 (m, 2H).

N-(4-methyl-2-nitrophenyl)pyridin-4-amine (12b). Orange oil. Yield: 55%; ^{1}H NMR (400 MHz, $CDCl_3$) δ 9.09 (s, 1H), 8.49 (d, J = 5.8 Hz, 2H), 8.03 (d, J = 1.1 Hz, 1H), 7.53 (d, J = 8.6 Hz, 1H), 7.38 (dd, J = 8.6, 2.0 Hz, 1H), 7.09 (dd, J = 4.8, 1.4 Hz, 2H), 2.45 – 2.35 (m, 3H).

General procedures for synthesis of compounds 12c-12f. To a mixture of nitrobenzene **11c-11d** (1.0 mmol) in toluene (10 mL) were added appropriate aniline (3.0 mmol), tris(dibenzylideneacetone)dipalladium ($Pd_2(dba)_3$, 92 mg, 0.1 mmol), BINAP (23 mg, 0.15 mmol) and cesium carbonate (650 mg, 2.0 mmol). The mixture was then stirred at 110^{o}C for 24 h under argon atmosphere. After cooling to room temperature, the mixture was filtered through a pad of celite and the filtrate was then concentrated in vacuo to afford a residue, which was purified by silica gel chromatography (petroleum/ethyl acetate, 50:1) to give compounds **12c-12f** as red oil.[59]

N-(4-methyl-2-nitrophenyl)tetrahydro-2H-pyran-4-amine (12c). Red oil. Yield: 65%; ^{1}H NMR (400 MHz, $CDCl_3$) δ 7.99 (s, 2H), 7.26 (d, J = 7.6 Hz, 1H), 6.80 (d, J = 8.8 Hz, 1H), 4.02 (dt, J = 11.8, 3.7 Hz, 2H), 3.77 – 3.67 (m, 1H), 3.58 (dd, J = 16.4, 6.0 Hz, 2H), 2.26 (s, 3H), 2.06 (d, J = 13.0 Hz, 2H), 1.69 (dd, J = 10.1, 3.9 Hz, 1H), 1.66 – 1.61 (m, 1H).

5-methyl-3-nitro-N-phenylpyridin-2-amine (12d). Red oil. Yield: 63%; ^{1}H NMR (400 MHz, $CDCl_3$) δ 10.01 (s, 1H), 8.34 (s, 2H), 7.64 (d, J = 8.0 Hz, 2H), 7.38 (t, J = 7.5 Hz, 2H), 7.16 (t, J = 7.4 Hz, 1H), 2.33 (s, 3H).

5-methyl-3-nitro-N-(pyridin-4-yl)pyridin-2-amine (12e). Red oil. Yield: 53%; ^{1}H NMR (400 MHz, $CDCl_3$) δ 10.13 (s, 1H), 8.51 (s, 2H), 8.43 (d, J = 9.0 Hz, 1H), 8.38 (d, J = 8.2 Hz, 1H), 7.69 (s, 2H), 2.38 (d, J = 9.1 Hz, 3H).

4-methyl-2-nitro-N-phenylaniline (12f). Red oil.Yield: 60%; ^{1}H NMR (400 MHz, $CDCl_3$) δ 9.36 (s, 1H), 8.00 (s, 1H), 7.39 (t, J = 7.8 Hz, 2H), 7.25 (d, J = 7.6 Hz, 2H), 7.23 – 7.15 (m, 3H), 2.29 (s, 3H).

General procedures for synthesis of compounds 13a-13f. To a mixture of **12a-12f** (1.0 mmol) in EtOH (10 mL) was added palladium hydroxide (238 mg, 1.0 mmol) and stirred at room temperature for 6 h under hydrogen atmosphere. The mixture was then filtered through a pad of celite. The filtrate was concentrated in vacuo to give a yellow solid, which was purified by silica gel chromatography (petroleum/ethyl acetate, 10:1) to give compounds **13a-13f** as colorless solid.

5-Fluoro-N²-(tetrahydro-2H-pyran-4-yl)pyridine-2,3-diamine (13a). Colorless solid.Yield: 83%; ^{1}H NMR (400 MHz, $CDCl_3$) δ 6.65 (dd, J = 8.5, 5.5 Hz, 1H), 6.51 – 6.41 (m, 2H), 4.02 (dt, J = 11.9, 3.7 Hz, 2H), 3.50 (td, J = 11.6, 2.3 Hz, 2H), 3.34 (tt, J = 10.2, 4.0 Hz, 1H), 2.03 – 1.96 (m, 2H), 1.57 – 1.46 (m, 2H).

4-Methyl-N¹-(pyridin-4-yl)benzene-1,2-diamine (13b). Colorless solid.Yield: 89%; ^{1}H NMR (400 MHz, $CDCl_3$) δ 8.24 (dd, J = 4.8, 1.5 Hz, 2H), 7.01 (d, J = 7.9 Hz, 1H), 6.67 (d, J = 1.1 Hz, 1H), 6.62 (dd, J = 7.9, 1.3 Hz, 1H), 6.53 (dd, J = 4.8, 1.5 Hz, 2H), 5.59 (s, 1H), 2.38 – 2.27 (m, 3H).

4-methyl-N¹-(tetrahydro-2H-pyran-4-yl)benzene-1,2-diamine (13c). Colorless solid. Yield: 50%; ^{1}H NMR (400 MHz, $CDCl_3$) δ 6.66 – 6.59 (m, 3H), 4.02 (dt, J = 11.9, 3.8 Hz, 2H), 3.52 (td, J = 11.5, 2.3 Hz, 2H), 3.42 (ddd, J = 10.2, 6.1, 4.2 Hz, 1H), 2.25 (s, 3H), 2.07 – 2.01 (m, 2H), 1.59 – 1.48 (m, 2H).

5-methyl-N²-(pyridin-4-yl)pyridine-2,3-diamine (13d). Colorless solid. Yield: 81%; ^{1}H NMR (400 MHz, $CDCl_3$) δ 8.30 (d, J = 5.3 Hz, 2H), 7.71 (s, 1H), 7.02 (d, J = 5.3 Hz, 2H), 6.91 (s, 1H), 6.63 (s, 1H), 2.25 (s, 3H).

5-Methyl-N²-phenylpyridine-2,3-diamine (13e). Colorless solid. Yield: 78%; ^{1}H NMR (400 MHz, $CDCl_3$) δ 7.69 (s, 1H), 7.28 (dd, J = 9.0, 6.8 Hz, 2H), 7.13 (d, J = 7.8 Hz, 2H), 6.93 (t, J = 7.3 Hz, 1H), 6.88 (s, 1H), 6.03 (s, 1H), 3.46 (s, 2H), 2.34 – 2.17 (m, 3H).

4-methyl-N¹-phenylbenzene-1,2-diamine (13f). Colorless solid. Yield: 55%; ^{1}H NMR (400 MHz, $CDCl_3$) δ 7.24 – 7.19 (m, 2H), 7.02 (d, J = 7.9 Hz, 1H), 6.85 – 6.79 (m, 1H), 6.74 – 6.70 (m, 2H), 6.66 (d, J = 1.0 Hz, 1H), 6.60 (dd, J = 7.9, 1.3 Hz, 1H), 5.11 (s, 1H), 3.76 (s, 2H), 2.32 (s, 3H).

Protein expression and purification. The pET15b-PDE10A plasmid for expression of the recombinant catalytic domain (residues 446-789) was subcloned and purified using previously reported protocols.[60] Briefly, the plasmid was transferred to *E. coli* strain BL21 (Codonplus, Stratagene). Then, the *E. coli* cells carrying the recombinant plasmid were grown in 2xYT medium (containing 100 μg/mL ampicillin and 30 μg/mL chloramphenicol) at 37 °C until an OD_{600} = 0.6-0.8 was achieved. Then, 1 mM isopropyl-*β*-D-thiogalactopyranoside was added to induce the expression of the PDE10A protein and the culture was incubated at 20 °C for 24 h. A nickel nitriloacetic acid (Ni-NTA) column (Qiagen) was used to purify PDE10A proteins. The concentration of the PDE10A fractions was estimated by monitoring the absorbance at 280 nm (calculated using the ProtParam software). A typical batch of purification yielded 100–200 mg of PDE10A protein from a 1.0 L cell culture. The catalytic domains of PDE2A (580-919), PDE3A (679-1087), PDE4D (86-413), PDE7A (130-482), PDE9A (181-506), PDE8A (480-820), PDE10A (449-770), and PDE11A (588-911) were purified using similar protocols, as previously reported.[60-64] PDE1C (2-634) and PDE6C (1−858) were

purchased from BPS Bioscience.

Enzymatic assays. The enzymatic activity of the catalytic domain of PDE10A2 was measured with ^{3}H-cGMP as the substrate in a buffer composed of 50 mM Tris, pH 7.5, 4 mM $MgCl_2$ and 1 mM dithiothreitol; 20,000 - 30,000 cpm ^{3}H-cGMP was used in each assay. Different concentrations of solubilized inhibitors in DMSO were added to the PDE10A enzyme. The enzymatic reaction was performed at room temperature for 15 min and then terminated by the addition of 0.2 M $ZnSO_4$. The reaction product was precipitated by the addition of 0.2 N $Ba(OH)_2$ and the unreacted ^{3}H-cGMP remained in the supernatant. The radioactivity in the supernatant was measured in 2.5 ml of Ultima Gold liquid scintillation cocktails (PerkinElmer) with a PerkinElmer 2910 liquid scintillation counter. At least eight concentrations of inhibitors were used to calculate the IC_{50} values of each inhibitor. Each measurement was repeated at least three times, and IC_{50} values were calculated using a nonlinear regression equation. The mean values of the measurements were considered the final IC_{50} values and reported with SD of the three or four measurements. In this assay, papaverine was used as the reference compound and determined to have an IC_{50} of 0.1 μM, which is comparable to the value ranging from 0.02 to 0.2 μM in the Binding Database (http://www.bindingdb.org).

Crystallization and structure refinement. The crystals of PDE10A2 were grown using the hanging drop method similar to those previously reported.[60-64] Briefly, the unliganded PDE10A2 enzyme (10 mg/mL in a buffer composed of 20 mM Tris-HCl (pH 7.5), 50 mM NaCl, 1 mM EDTA and 1 mM β-mercaptoethanol) was vapor-diffused against the well buffer of 0.1 M Hepes (pH 7.5), 0.2 M $MgCl_2$, 18% PEG3350 and 50 mM 2-mercaptoethanol. The complex of PDE10A2 with **AF-399/14387019** or compound **2b** was prepared by soaking the unliganded crystals in 20 mM **AF-399/14387019** or compound **2b** in a buffer of 0.1 M Hepes (pH 7.5), 0.1 M $MgCl_2$, 16% PEG 8000 and 60 mM 2-ME at 4 °C for 24 h. The crystallization buffer containing 20% ethylene glycol was used as the cryosolvent. Diffraction data were collected at 100 K on an in-house Oxford Diffraction Xcalibur Nova diffractometer. The data were processed using the program *CrysAlis Pro* and the structures were solved and refined using CCP4.[65] The coordinates and structure factors have been deposited in the Protein Data Bank with PDB ID of 6IJH and 6IJI. Data collection and refinement statistics for all structures were shown in supporting information.

Pharmacokinetics analysis of 2b. The pharmacokinetic properties of **2b** were analyzed by the Medicilon Company, Shanghai, China. Three male SD rats with a body weight of 230-260 g were purchased from Shanghai SIPPR-BK LAB Animal Ltd., Shanghai, China, and used for the

pharmacokinetic analysis of **2b**. It was dissolved/suspended in 5% DMSO, 10% Solutol, and 85% water for intravenous administration (i.v.). A final dosage of 2.5 mg/kg rat of the formulated compound was administered for i.v. purpose, and the blood samples were taken at various time points during a 24 h period. The concentration of compounds in the blood was analyzed by LC-MS/MS (Shimadzu liquid chromatographic system and API4000 mass spectrometer, Applied Biosystems, Ontario, Canada).

Pharmacodynamics effects of compound 2b against PAH in Wistar rats. All animal care procedures and experimental protocols[61,62] were performed in accordance with the "Guide for the Care and Use of Laboratory Animals" (National Institutes of Health Publication, revised 1996, No. 86-23, Bethesda, MD) and approved by the Institutional Ethical Committee for Animal Research of Sun Yat-sen University. Forty Wistar rats (6-7 weeks, 180-220 g) were purchased from the Laboratory Animal Center of Southern Medical University (Guangzhou, China) and used to evaluate the anti-PAH effects of compound **2b** on PAH. The rats were randomly divided into four groups as follows: control, model, compound **2b** (2.5 mg/kg), and positive control (sildenafil citrate, 10 mg/kg). The rats were maintained on a 12 h light/dark cycle (light from 7:00 to 19:00) at 24 ± 1 °C and 60−70% relative humidity. Sterile food and water were provided according to the institutional guidelines. Prior to each experiment, the rats were fasted overnight and allowed free access to water. All rats were administered MCT 60 mg/kg, except for the control group. Then, the rats were treated daily with the drug vehicle (control and model groups), **2b** (2.5 mg/kg, i.p.), and sildenafil citrate (10 mg/kg, p.o.) for 3 weeks. **2b** and sildenafil citrate were dissolved in 5% DMSO/10% Solutol/85% water solution and administered 0.4 mL per 100 g weight. Rats were anesthetized with pentobarbital sodium (60 mg/kg, i.p.). Mean pulmonary artery pressure (mPAP) was measured by right heart catheterization. Following pressure measurement, the heart was divided and the atria dissected. The weight of right ventricle (RV) and left ventricle plus ventricular septum (LV+S) was measured, and RV/(LV+S) ratio was taken as right ventricular hypertrophy index (RVHI). Then a part of lung tissues were taken and fixed with 4% paraformaldehyde. Routine HE staining was performed to observe the pathological changes and calculate the percentage (WT %) of the medial wall thickness of pulmonary arterioles. The concentrations of cAMP and cGMP were measured with Abbkine and Cayman ELISA kits according to the manufacturers' instructions, respectively.

VSMC culture. Human pulmonary artery smooth muscle cells (HPASMCs) were obtained from BeNa Culture Collection (Beijing, China). HPASMCs were cultured in Dulbecco's modified Eagle's medium (high glucose) (HDMEM) with 10% fetal bovine serum (FBS, Hyclone, Logan, UT, USA), penicillin (100 IU/ml) and streptomycin (100 mg/ml) at 37 °C in a 5% CO_2 humidified incubator. Cells in the four to eight passages were used, and cells at 80–90% confluence were arrested by incubating in serum-deprived DMEM for 12 h before intervention. PDGF-BB (20 μM) was treated for 24 h. PDE10A inhibitor **2b** and PF-2545920 were added 2 h after the addition of PDGF-BB and were incubated for 22 h.

Western blot analysis. Cells were homogenized in lysis buffer, and the supernatant was extracted for the measurement of total protein with a protein assay kit (BCA; Pierce, Santa Cruz, CA, USA). Equal amounts of total protein were separated in SDS-PAGE, and transferred to PVDF membranes in Trisglycine methanol buffer. The bands were visualized using the enhanced chemiluminescent. The primary antibodies against OPN, PCNA, $SM22_{\alpha}$ and α-tubulin were purchased from Proteintech (Wuhan, China). Antibodies against α-SMA was obtained from Abcam (Cambridge, MA, USA).

■ ASSOCIATED CONTENT

Supporting Information

Detailed protocols for molecular dynamics-based virtual screening, Diffraction data and structure refinement statistics of crystallography, Extended data series for tested compounds appear in the Supporting Information. This material is available free of charge *via* the Internet.

Molecular formula strings (CSV)

Accession Codes

The atomic coordinates and structure factors have been deposited into the RCSB Protein Data Bank with accession numbers of 6IJH and 6IJI. Authors will release the atomic coordinates and experimental data upon article publication.

■ AUTHOR INFORMATION

Corresponding Authors

* E-mail: wudeyan3@mail.sysu.edu.cn (W.D. Wu), wyinuo3@mail.sysu.edu.cn (W.Y. Wu), and

luohb77@mail.sysu.edu.cn (H.-B. Luo); Fax: +86-20-3994 3000

ORCID

Hai-Bin Luo: 0000-0002-2163-0509

Deyan Wu: 0000-0001-5855-8662

Yinuo Wu: 0000-0003-3071-5333

Yi-you Huang: 0000-0002-0712-1310

Author Contributions

‖ These authors contributed equally to this work.

Notes

The authors declare no competing financial interest.

ABBREVIATIONS USED

BINAP, (±)-2,2'-bis(diphenylphosphino)-1,1'-binaphthyl; cAMP, cyclic adenosine monophosphate; cGMP, cyclic guanosine monophosphate; CNS, central nervous system; DMF, N,N-dimethylformamide; DMSO, dimethyl sulfoxide; DIPEA, N,N-diisopropylethylamine; HATU, 2-(7-Azabenzotriazol-1-yl)-N,N,N',N'-tetramethyluronium hexafluorophosphate; IC_{50}, half maximal inhibitory concentration; MD, molecular dynamics; MCT, monocrotaline; mPAP, mean pulmonary artery pressure; PAH, pulmonary arterial hypertension; PDE, phosphodiesterase; PDE10, phosphodiesterase-10; RVHI, right ventricle hypertrophy index; SPBG, selective pocket binding group; TLC, thin layer chromatography; TMS, tetramethylsilane; WT, wall thickness.

■ ACKNOWLEDGEMENTS

We cordially thank anonymous reviewers' valuable comments and kind proofreading of the manuscript. This work was supported by Natural Science Foundation of China (21572279, 21877134, 81872727, 81602955, and 81703341), Science Foundation of Guangdong Province (2016A030310144), Pearl River S&T Nova program of Guangzhou (201806010190), The Fundamental Research Funds for the Central Universities (Sun Yat-Sen University) (No. 17ykjc03 and 17ykpy20), Guangdong Province Higher Vocational Colleges & Schools Pearl River Scholar Funded Scheme (2016). We cordially thank Prof. H. Ke from Department of Biochemistry and Biophysics at the University of North Carolina, Chapel Hill, for his proofreading and his help with molecular cloning, expression, purification, crystal structure, and bioassay of PDEs. We cordially thank Dr. Zhengchao Tu from

Guangzhou Institutes of Biomedicine and Health and Zhiping Zeng from Xiamen University for their help to screen the binding affinities of compound **2b** against twenty different targets.

■ References

(1) Beavo, J. A. Cyclic Nucleotide Phosphodiesterases: Functional Implications of Multiple Isoforms. *Physiol. Rev.* **1995,** *75*, 725-748.

(2) Bender, A. T.; Beavo, J. A. Cyclic Nucleotide Phosphodiesterases: Molecular Regulation to Clinical Use. *Pharmacol. Rev.* **2006,** *58*, 488-520.

(3) Lakics, V.; Karran, E. H.; Boess, F. G. Quantitative Comparison of Phosphodiesterase mRNA Distribution in Human Brain and Peripheral Tissues. *Neuropharmacology* **2010,** *59*, 367-374.

(4) Helal, C. J.; Kang, Z. J.; Hou, X. J.; Pandit, J.; Chappie, T. A.; Humphrey, J. M.; Marr, E. S.; Fennell, K. F.; Chenard, L. K.; Fox, C.; Schmidt, C. J.; Williams, R. D.; Chapin, D. S.; Siuciak, J.; Lebel, L.; Menniti, F.; Cianfrogna, J.; Fonseca, K. R.; Nelson, F. R.; O'Connor, R.; MacDougall, M.; McDowell, L.; Liras, S. Use of Structure-Based Design to Discover a Potent, Selective, in Vivo Active Phosphodiesterase 10A Inhibitor Lead Series for the Treatment of Schizophrenia. *J. Med. Chem.* **2011,** *54*, 4536-4547.

(5) Chappie, T. A.; Helal, C. J.; Hou, X. J. Current Landscape of Phosphodiesterase 10A (PDE10A) Inhibition. *J. Med. Chem.* **2012,** *55*, 7299-7331.

(6) Kehler, J. Phosphodiesterase 10A Inhibitors: A 2009-2012 Patent Update. *Expert Opin. Ther. Pat.* **2013,** *23*, 31-45.

(7) Bartolome-Nebreda, J. M.; Conde-Ceide, S.; Garcia, M. Phosphodiesterase 10A Inhibitors: Analysis of US/EP Patents Granted Since 2012. *Pharm. Pat. Anal.* **2015,** *4*, 161-186.

(8) Zagorska, A.; Partyka, A.; Bucki, A.; Gawalskax, A.; Czopek, A.; Pawlowski, M. Phosphodiesterase 10 Inhibitors - Novel Perspectives for Psychiatric and Neurodegenerative Drug Discovery. *Curr. Med. Chem.* **2018,** *25*, 3455-3481.

(9) Humbert, M.; Sitbon, O.; Chaouat, A.; Bertocchi, M.; Habib, G.; Gressin, V.; Yaici, A.; Weitzenblum, E.; Cordier, J. F.; Chabot, F.; Dromer, C.; Pison, C.; Reynaud-Gaubert, M.; Haloun, A.; Laurent, M.; Hachulla, E.; Cottin, V.; Degano, B.; Jais, X.; Montani, D.; Souza, R.; Simonneau, G. Survival in Patients with Idiopathic, Familial, and Anorexigen-associated Pulmonary Arterial Hypertension in the Modern Management Era. *Circulation* **2010,** *122*, 156-163.

(10) Benza, R. L.; Miller, D. P.; Barst, R. J.; Badesch, D. B.; Frost, A. E.; McGoon, M. D. An Evaluation of Long-Term Survival from Time of Diagnosis in Pulmonary Arterial Hypertension from the REVEAL Registry. *Chest* **2012,** *142*, 448-456.

(11) Tian, X.; Vroom, C.; Ghofrani, H. A.; Weissmann, N.; Bieniek, E.; Grimminger, F.; Seeger, W.; Schermuly, R. T.; Pullamsetti, S. S. Phosphodiesterase 10A Upregulation Contributes to Pulmonary Vascular Remodeling. *Plos One* **2011,** *6*, e18136.

(12) Farber, H. W.; Loscalzo, J. Mechanisms of Disease: Pulmonary Arterial Hypertension. *New Engl. J. Med.* **2004,** *351*, 1655-1665.

(13) Fujishige, K.; Kotera, J.; Michibata, H.; Yuasa, K.; Takebayashi, S.; Okumura, K.; Omori, K. Cloning and Characterization of a Novel Human Phosphodiesterase that Hydrolyzes both cAMP and cGMP (PDE10A). *J. Biol. Chem.* **1999,** *274*, 18438-18445.

(14) Soderling, S. H.; Bayuga, S. J.; Beavo, J. A. Isolation and Characterization of a Dual-Substrate Phosphodiesterase Gene Family: PDE10A. *Proc. Natl. Acad. Sci. USA* **1999,** *96*, 7071-7076.

(15) Schermuly, R. T.; Pullamsetti, S. S.; Kwapiszewska, G.; Dumitrascu, R.; Tian, X.; Weissmann, N.; Ghofrani, H. A.; Kaulen, C.; Dunkern, T.; Schudt, C.; Voswinckel, R.; Zhou, J.; Samidurai, A.; Klepetko, W.; Paddenberg, R.; Kummer, W.; Seeger, W.; Grimminger, F. Phosphodiesterase 1 Upregulation in Pulmonary Arterial Hypertension Target for Reverse-Remodeling Therapy. *Circulation* **2007,** *115*, 2331-2339.

(16) Bubb, K. J.; Trinder, S. L.; Baliga, R. S.; Patel, J.; Clapp, L. H.; MacAllister, R. J.; Hobbs, A. J. Inhibition of Phosphodiesterase 2 Augments cGMP and cAMP Signaling to Ameliorate Pulmonary Hypertension. *Circulation* **2014,** *130*, 496-507.

(17) Pullamsetti, S. S.; Savai, R.; Schaefer, M. B.; Wilhelm, J.; Ghofrani, H. A.; Weissmann, N.; Schudt, C.; Fleming, I.; Mayer, K.; Leiper, J.; Seeger, W.; Grimminger, F.; Schermuly, R. T. cAMP Phosphodiesterase Inhibitors Increases Nitric Oxide Production by Modulating Dimethylarginine Dimethylaminohydrolases. *Circulation* **2011,** *123*, 1194-1204.

(18) Takase, Y.; Saeki, T.; Fujimoto, M.; Saito, I. Cyclic GMP Phosphodiesterase Inhibitors. 1. The Discovery of a Novel Potent Inhibitor, 4-((3,4-(Methylenedioxy)benzyl)amino)-6,7,8-trimethoxyquinazoline. *J. Med. Chem.* **1993,** *36*, 3765-3770.

(19) Lipinski, C. A.; Lombardo, F.; Dominy, B. W.; Feeney, P. J. Experimental and Computational Approaches to Estimate Solubility and Permeability in Drug Discovery and Development Settings. *Adv. Drug Deliv. Rev.* **2001,** *46*, 3-26.

(20) Rester, U. From Virtuality to Reality - Virtual Screening in Lead Discovery and Lead Optimization: A Medicinal Chemistry Perspective. *Curr. Opin. Drug Disc.* **2008,** *11*, 559-568.

(21) Baell, J. B.; Holloway, G. A. New Substructure Filters for Removal of Pan Assay Interference Compounds (PAINS) from Screening Libraries and for Their Exclusion in Bioassays. *J. Med. Chem.* **2010,** *53*, 2719-2740.

(22) Verhoest, P. R.; Chapin, D. S.; Corman, M.; Fonseca, K.; Harms, J. F.; Hou, X. J.; Marr, E. S.; Menniti, F. S.; Nelson, F.; O'Connor, R.; Pandit, J.; Proulx-LaFrance, C.; Schmidt, A. W.; Schmidt, C. J.; Suiciak, J. A.; Liras, S. Discovery of a Novel Class of Phosphodiesterase 10A Inhibitors and Identification of Clinical Candidate 2-[4-(1-Methyl-4-pyridin-4-yl-1H-pyrazol-3-yl)-phenoxymethyl] -quinoline (PF-2545920) for the Treatment of Schizophrenia. *J. Med. Chem.* **2009,** *52*, 5188-5196.

(23) Massova, I.; Kollman, P. A. Combined Molecular Mechanical and Continuum Solvent Approach (MM-PBSA/GBSA) to Predict Ligand Binding. *Perspect. Drug Discov.* **2000,** *18*, 113-135.

(24) Hou, T. J.; Wang, J. M.; Li, Y. Y.; Wang, W. Assessing the Performance of the MM/PBSA and MM/GBSA Methods. 1. The Accuracy of Binding Free Energy Calculations Based on Molecular Dynamics Simulations. *J. Chem. Inf. Model.* **2011,** *51*, 69-82.

(25) Chino, A.; Masuda, N.; Amano, Y.; Honbou, K.; Mihara, T.; Yamazaki, M.; Tomishima, M. Novel Benzimidazole Derivatives as Phosphodiesterase 10A (PDE10A) Inhibitors with Improved Metabolic Stability. *Bioorg. Med. Chem.* **2014,** *22*, 3515-3526.

(26) Kehler, J.; Ritzen, A.; Langgard, M.; Petersen, S. L.; Farah, M. M.; Bundgaard, C.; Christoffersen, C. T.; Nielsen, J.; Kilburn, J. P. Triazoloquinazolines as a Novel Class of Phosphodiesterase 10A (PDE10A) Inhibitors. *Bioorg. Med. Chem. Lett.* **2011,** *21*, 3738-3742.

(27) Bartolome-Nebreda, J. M.; Delgado, F.; Martin-Martin, M. L.; Martinez-Viturro, C. M.; Pastor, J.; Tong, H. M.; Iturrino, L.; Macdonald, G. J.; Sanderson, W.; Megens, A.; Langlois, X.; Somers, M.; Vanhoof, G.; Conde-Ceide, S. Discovery of a Potent, Selective, and Orally Active Phosphodiesterase 10A Inhibitor for the Potential Treatment of Schizophrenia. *J. Med. Chem.* **2014,** *57*, 4196-4212.

(28) Hu, E.; Andrews, K.; Chmait, S.; Zhao, X.; Davis, C.; Miller, S.; Hill Della Puppa, G.; Dovlatyan, M.; Chen, H.; Lester-Zeiner, D.; Able, J.; Biorn, C.; Ma, J.; Shi, J.; Treanor, J.; Allen, J. R. Discovery of Novel Imidazo[4,5-b]pyridines as Potent and Selective Inhibitors of Phosphodiesterase 10A (PDE10A). *ACS Med. Chem. Lett.* **2014,** *5*, 700-705.

(29) Burdi, D. F.; Campbell, J. E.; Wang, J.; Zhao, S.; Zhong, H.; Wei, J.; Campbell, U.; Shao, L.; Herman, L.; Koch, P.; Jones, P. G.; Hewitt, M. C. Evolution and Synthesis of Novel Orally Bioavailable Inhibitors of PDE10A. *Bioorg. Med. Chem. Lett.* **2015,** *25*, 1864-1868.

(30) Meegalla, S. K.; Huang, H.; Illig, C. R.; Parks, D. J.; Chen, J. S.; Lee, Y. K.; Wilson, K. J.; Patel, S. K.; Cheung, W. S.; Lu, T. B.; Kirchner, T.; Askari, H. B.; Geisler, J.; Patch, R. J.; Gibbs, A. C.; Rady, B.; Connelly, M.; Player, M. R. Discovery of Novel Potent Imidazo[1,2-b]pyridazine PDE10A Inhibitors. *Bioorg. Med. Chem. Lett.* **2016,** *26*, 4216-4222.

(31) Cox, C. D.; Hostetler, E. D.; Flores, B. A.; Evelhoch, J. L.; Fan, H.; Gantert, L.; Holahan, M.; Eng, W. S.; Joshi, A.; McGaughey, G.; Meng, X. J.; Purcell, M.; Raheem, I. T.; Riffel, K.; Yan, Y. W.; Renger, J. J.; Smith, S. M.; Coleman, P. J. Discovery of [C-11]MK-8193 as a PET Tracer to Measure Target Engagement of Phosphodiesterase 10A (PDE10A) Inhibitors. *Bioorg. Med. Chem. Lett.* **2015,** *25*, 4893-4898.

(32) Chappie, T. A.; Humphrey, J. M.; Allen, M. P.; Estep, K. G.; Fox, C. B.; Lebel, L. A.; Liras, S.; Marr, E. S.; Menniti, F. S.; Pandit, J.; Schmidt, C. J.; Tu, M. H.; Williams, R. D.; Yang, F. V. Discovery of a Series of 6,7-Dimethoxy-4-pyrrolidylquinazoline PDE10A Inhibitors. *J. Med. Chem.* **2007,** *50*, 182-185.

(33) Kunitomo, J.; Yoshikawa, M.; Fushimi, M.; Kawada, A.; Quinn, J. F.; Oki, H.; Kokubo, H.; Kondo, M.; Nakashima, K.; Kamiguchi, N.; Suzuki, K.; Kimura, H.; Taniguchi, T. Discovery of 142-Fluoro-4-(1H-pyrazol-1-yl)phenyl]-5-methoxy-3-(1phenyl-1H-pyrazol-5-yl)pyridazin-4(1H)-one (TAK-063), a Highly Potent, Selective, and Orally Active Phosphodiesterase 10A (PDE10A) Inhibitor. *J. Med. Chem.* **2014,** *57*, 9627-9643.

(34) Hamaguchi, W.; Masuda, N.; Isomura, M.; Miyamoto, S.; Kikuchi, S.; Amano, Y.; Honbou, K.; Mihara, T.; Watanabe, T. Design and Synthesis of Novel Benzimidazole Derivatives as Phosphodiesterase 10A Inhibitors with Reduced CYP1A2 Inhibition. *Bioorg. Med. Chem.* **2013,** *21*, 7612-7623.

(35) Hu, E.; Kunz, R. K.; Chen, N.; Rumfelt, S.; Siegmund, A.; Andrews, K.; Chmait, S.; Zhao, S.; Davis, C.; Chen, H.; Lester-Zeiner, D.; Ma, J.; Biorn, C.; Shi, J. X.; Porter, A.; Treanor, J.; Allen, J. R. Design, Optimization, and Biological Evaluation of Novel Keto-benzimidazoles as Potent and Selective Inhibitors of Phosphodiesterase 10A (PDE10A). *J. Med. Chem.* **2013,** *56*, 8781-8792.

(36) Shipe, W. D.; Sharik, S. S.; Barrow, J. C.; McGaughey, G. B.; Theberge, C. R.; Uslaner, J. M.; Yan, Y. W.; Renger, J. J.; Smith, S. M.; Coleman, P. J.; Cox, C. D. Discovery and Optimization of a Series of Pyrimidine-Based Phosphodiesterase 10A (PDE10A) Inhibitors Through Fragment Screening, Structure-Based Design, and Parallel Synthesis. *J. Med. Chem.* **2015,** *58*, 7888-7894.

(37) Hu, E.; Chen, N.; Bourbeau, M. P.; Harrington, P. E.; Biswas, K.; Kunz, R. K.; Andrews, K. L.; Chmait, S.; Zhao, X. N.; Davis, C.; Ma, J.; Shi, J. X.; Lester-Zeiner, D.; Danao, J.; Able, J.; Cueva, M.; Talreja, S.; Kornecook, T.; Chen, H.; Porter, A.; Hungate, R.; Treanor, J.; Allen, J. R. Discovery of Clinical Candidate 1-(4-(3-(4-(1H-benzo[d]imidazole-2-carbonyl)phenoxy)pyrazin-2-yl)piperidin-1-yl)ethanone (AMG 579), a Potent, Selective, and Efficacious Inhibitor of Phosphodiesterase 10A (PDE10A). *J. Med. Chem.* **2014,** *57*, 6632-6641.

(38) Yoshikawa, M.; Hitaka, T.; Hasui, T.; Fushimi, M.; Kunitomo, J.; Kokubo, H.; Oki, H.; Nakashima, K.; Taniguchi, T. Design and Synthesis of Potent and Selective Pyridazin-4(1H)-one-based PDE10A Inhibitors Interacting with Tyr683 in the PDE10A Selectivity Pocket. *Bioorg. Med. Chem.* **2016,** *24*, 3447-3455.

(39) Raheem, I. T.; Schreier, J. D.; Fuerst, J.; Gantert, L.; Hostetler, E. D.; Huszar, S.; Joshi, A.; Kandebo, M.; Kim, S. H.; Li, J.; Ma, B.; McGaughey, G.; Sharma, S.; Shipe, W. D.; Uslaner, J.; Vandeveer, G. H.; Yan, Y. W.; Renger, J. J.; Smith, S. M.; Coleman, P. J.; Cox, C. D. Discovery of Pyrazolopyrimidine Phosphodiesterase 10A Inhibitors for the Treatment of Schizophrenia. *Bioorg. Med. Chem. Lett.* **2016,** *26*, 126-132.

(40) Peng, L.; Gao, X.; Duan, L.; Ren, X.; Wu, D.; Ding, K. Identification of Pyrido[1,2-α]pyrimidine-4-ones as New Molecules Improving the Transcriptional Functions of Estrogen-Related Receptor α. *J. Med. Chem.* **2011,** *54*, 7729-7733.

(41) Karaman, M. W.; Herrgard, S.; Treiber, D. K.; Gallant, P.; Atteridge, C. E.; Campbell, B. T.; Chan, K. W.; Ciceri, P.; Davis, M. I.; Edeen, P. T.; Faraoni, R.; Floyd, M.; Hunt, J. P.; Lockhart, D. J.; Milanov, Z. V.; Morrison, M. J.; Pallares, G.; Patel, H. K.; Pritchard, S.; Wodicka, L. M.; Zarrinkar, P. P., A Quantitative Analysis of Kinase Inhibitor Selectivity. *Nat. Biotech.* **2008,** *26*, 127-132.

(42) Ren, X.; Pan, X.; Zhang, Z.; Wang, D.; Lu, X.; Li, Y.; Wen, D.; Long, H.; Luo, J.; Feng, Y.; Zhuang, X.; Zhang, F.; Liu, J.; Leng, F.; Lang, X.; Bai, Y.; She, M.; Tu, Z.; Pan, J.; Ding, K. Identification of GZD824 as An Orally Bioavailable Inhibitor that Targets Phosphorylated and Nonphosphorylated Breakpoint Cluster Region–Abelson (Bcr-Abl) Kinase and Overcomes Clinically Acquired Mutation-Induced Resistance Against Imatinib. *J. Med. Chem.* **2013,** *56*, 879-894.

(43) Wang, Z.; Zhang, Y.; Pinkas, D. M.; Fox, A. E.; Luo, J.; Huang, H.; Cui, S.; Xiang, Q.; Xu, T.; Xun, Q.; Zhu, D.; Tu, Z.; Ren, X.; Brekken, R. A.; Bullock, A. N.; Liang, G.; Ding, K.; Lu, X. Design, Synthesis, and Bological Evaluation of 3-(Imidazo [1, 2-a] pyrazin-3-ylethynyl)-4-isopropyl-N-(3-((4-

methylpiperazin-1-yl) methyl)-5-(trifluoromethyl)phenyl) benzamide as A Dual Inhibitor of Discoidin Domain Receptors 1 and 2. *J. Med. Chem.* **2018**, *61*, 7977-7990.

(44) Gao, M.; Duan, L.; Luo, J.; Zhang, L.; Lu, X.; Zhang, Y.; Zhang, Z.; Tu, Z.; Xu, Y.; Ren, X.; Ding, K. Discovery and Optimization of 3-(2-(Pyrazolo[1, 5-a] pyrimidin-6-yl)ethynyl)benzamides as Novel Selective and Orally Bioavailable Discoidin Domain Receptor 1 (DDR1) Inhibitors. *J. Med. Chem.* **2013**, *56*, 3281-3295.

(45) Yao, Y.; Tu, Z.; Liao, C.; Wang, Z.; Li, S.; Yao, H.; Li, Z.; Jiang, S. Discovery of Novel Class I Histone Deacetylase Inhibitors with Promising in Vitro and in Vivo Antitumor Activities. *J. Med. Chem.* **2015,** *58*, 7672-7680.

(46) Yu, Y.; Huang, Y.; Zhang, C.; Wu, X.; Zhou, Q.; Wu, D.; Wu, Y.; Luo, H.-B. Discovery of Novel Pyrazolopyrimidinone Derivatives as Phosphodiesterase 9A Inhibitors Capable of Inhibiting Butyrylcholinesterase for Treatment of Alzheimer's Disease. *ACS Chem. Neurosci.* **2017,** *8*, 2522-2534.

(47) Zhu, J.; Yang, Q. Q.; Dai, D. D.; Huang, Q. X-ray Crystal Structure of Phosphodiesterase 2 in Complex with a Highly Selective, Nanomolar Inhibitor Reveals a Binding-Induced Pocket Important for Selectivity. *J. Am. Chem. Soc.* **2013,** *135*, 11708-11711.

(48) Burgin, A. B.; Magnusson, O. T.; Singh, J.; Witte, P.; Staker, B. L.; Bjornsson, J. M.; Thorsteinsdottir, M.; Hrafnsdottir, S.; Hagen, T.; Kiselyov, A. S.; Stewart, L. J.; Gurney, M. E. Design of Phosphodiesterase 4D (PDE4D) Allosteric Modulators for Enhancing Cognition with Improved Safety. *Nat. Biotechnol.* **2010,** *28*, 63-70.

(49) Huang, Y. Y.; Li, Z.; Cai, Y. H.; Feng, L. J.; Wu, Y.; Li, X.; Luo, H.-B. The Molecular Basis for the Selectivity of Tadalafil Toward Phosphodiesterase 5 and 6: A Modeling Study. *J. Chem. Inf. Model.* **2013,** *53*, 3044-3053.

(50) Shi, N.; Chen, S. Y. Mechanisms Simultaneously Regulate Smooth Muscle Proliferation and Differentiation. *J. Biomed. Res.* **2014**,*28*, 40-46.

(51) Sun, H. J.; Ren, X. S.; Xiong, X. Q.; Chen, Y. Z.; Zhao, M. X.; Wang, J. J.; Zhou, Y. B.; Han, Y.; Chen, Q.; Li, Y. H.; Kang, Y. M.; Zhu, G. Q. NLRP3 Inflammasome Activation Contributes to VSMC Phenotypic Transformation and Proliferation in Hypertension. *Cell Death Dis.* **2017**,*8*, e3074.

(52) Breslin, H. J.; Diamond, C. J.; Kavash, R. W.; Cai, C. Z.; Dyatkin, A. B.; Miskowski, T. A.; Zhang, S. P.; Wade, P. R.; Hornby, P. J.; He, W. Identification of a Dual Delta OR Antagonist/mu OR

Agonist as a Potential Therapeutic for Diarrhea-Predominant Irritable Bowel Syndrome (IBS-d). *Bioorg. Med. Chem. Lett.* **2012,** *22*, 4869-4872.

(53) Laronze-Cochard, M.; Kim, Y. M.; Brassart, B.; Riou, J. F.; Laronze, J. Y.; Sapi, J. Synthesis and Biological Evaluation of Novel 4,5-Bis(dialkylaminoalkyl)-substituted Acridines as Potent Telomeric G-quadruplex Ligands. *Eur. J. Med. Chem.* **2009,** *44*, 3880-3888.

(54) Carole, D.; Michel, D.; Julien, C.; Florence, D.; Anna, N.; Severine, J.; Gerard, D.; Pierre, T. D.; Jean-Pierre, G. Synthesis and Antileishmanial Activities of 4,5-Di-substituted Acridines as Compared to Their 4-Mono-substituted Homologues. *Bioorg. Med. Chem.* **2005,** *13*, 5560-5568.

(55) Escudero, M. I.; Kremenchuzky, L. D.; Perillo, I. A.; Cerecetto, H.; Blanco, M. M. Efficient Cesium Carbonate Promoted N-alkylations of Aromatic Cyclic Imides Under Microwave Irradiation. *Synthesis-Stuttgart* **2011**, 571-576.

(56) Howard, H. J.; Andrew, S. B.; Simon, S. N.; Pham, T. Y.; Roger, R. J.; Deborah, V.; Melissa, S. J.; Timothy, P. Heteroaryl Antagonists of Prostaglandin D2 Receptors. US, *WO2010037054*, **2010**.

(57) Kamal, A.; Ramu, R.; Tekumalla, V.; Khanna, G. B. R.; Barkume, M. S.; Juvekar, A. S.; Zingde, S. M. Remarkable DNA Binding Affinity and Potential Anticancer Activity of Pyrrolo[2,1-c][1,4]benzodiazepine-naphthalimide Conjugates Linked Through Piperazine Side-armed Alkane Spacers. *Bioorg. Med. Chem.* **2008,** *16*, 7218-7224.

(58) Cesari, N.; Biancalani, C.; Vergelli, C.; Dal Piaz, V.; Graziano, A.; Biagini, P.; Ghelardini, C.; Galeotti, N.; Giovannoni, M. P. Arylpiperazinylalkylpyridazinones and Analogues as Potent and Orally Active Antinociceptive Agents: Synthesis and Studies on Mechanism of Action. *J. Med. Chem.* **2006,** *49*, 7826-7835.

(59) Chino, A.; Masuda, N.; Amano, Y.; Honbou, K.; Mihara, T.; Yamazaki, M.; Tomishima M., Novel Benzimidazole Derivatives as Phosphodiesterase 10A (PDE10A) Inhibitors with Improved Metabolic Stability. *Bioorg. Med. Chem.* **2014,** *22*, 3515-3526.

(60) Wang, H. C.; Liu, Y. D.; Hou, J.; Zheng, M. Y.; Robinson, H.; Ke, H. M. Structural Insight into Substrate Specificity of Phosphodiesterase 10. *Proc. Natl. Acad. Sci. USA* **2007,** *104*, 5782-5787.

(61) Wu, D.; Zhang, T.; Chen, Y.; Huang, Y. D.; Geng, H.; Yu, Y.; Zhang, C.; Lai, Z.; Wu, Y.; Guo, X.; Chen, J.; Luo, H.-B. Discovery and Optimization of Chromeno[2,3-c]pyrrol-9(2H)-ones as Novel Selective and Orally Bioavailable Phosphodiesterase 5 Inhibitors for the Treatment of Pulmonary Arterial Hypertension. *J. Med. Chem.* **2017,** *60*, 6622-6637.

(62) Wu, D.; Huang, Y. D.; Chen, Y.; Huang, Y. Y.; Geng, H.; Zhang, T.; Zhang, C.; Li, Z.; Guo, L.; Chen, J. W.; Luo, H.-B. Optimization of Chromeno[2,3-c]pyrrol-9(2H)-ones as Highly Potent, Selective, and Orally Bioavailable PDE5 Inhibitors: Structure-Activity Relationship, X-ray Crystal Structure, and Pharmacodynamic Effect on Pulmonary Arterial Hypertension. *J. Med. Chem.,* **2018**, 61, 8468−8473.

(63) Huang, Y. Y.; Liu, X.; Wu, D. Y.; Tang, G. H.; Lai, Z. W.; Zheng, X. H.; Yin, S.; Luo, H.-B. The Discovery, Complex Crystal Structure, and Recognition Mechanism of a Novel Natural PDE4 Inhibitor from Selaginella Pulvinata. *Biochem. Pharmacol.* **2017,** *130*, 51-59.

(64) Shao, Y. X.; Huang, M.; Cui, W.; Feng, L. J.; Wu, Y.; Cai, Y.; Li, Z.; Zhu, X.; Liu, P.; Wan, Y.; Ke, H.; Luo, H.-B. Discovery of a Phosphodiesterase 9A Inhibitor as a Potential Hypoglycemic Agent. *J. Med. Chem.,* **2014**, *57*, 10304-10313.

(65) Winn, M. D.; Ballard, C. C.; Cowtan, K. D.; Dodson, E. J.; Emsley, P.; Evans, P. R.; Keegan, R. M.; Krissinel, E. B.; Leslie, A. G. W.; McCoy, A.; McNicholas, S. J.; Murshudov, G. N.; Pannu, N. S.; Potterton, E. A.; Powell, H. R.; Read, R. J.; Vagin, A.; Wilson, K. S. Overview of the CCP4 Suite and Current Developments. *Acta Crystallogr.* **2011,** *67*, 235-242.

TOC Graphic

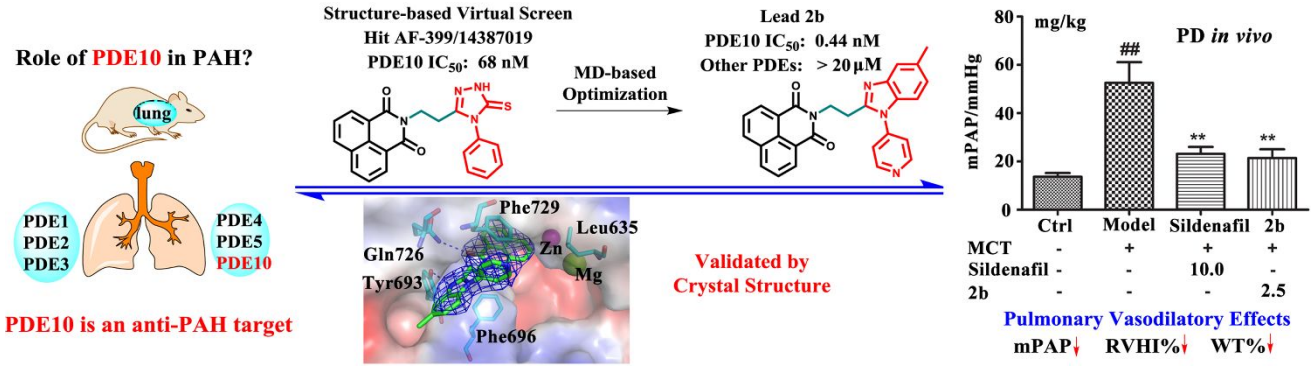

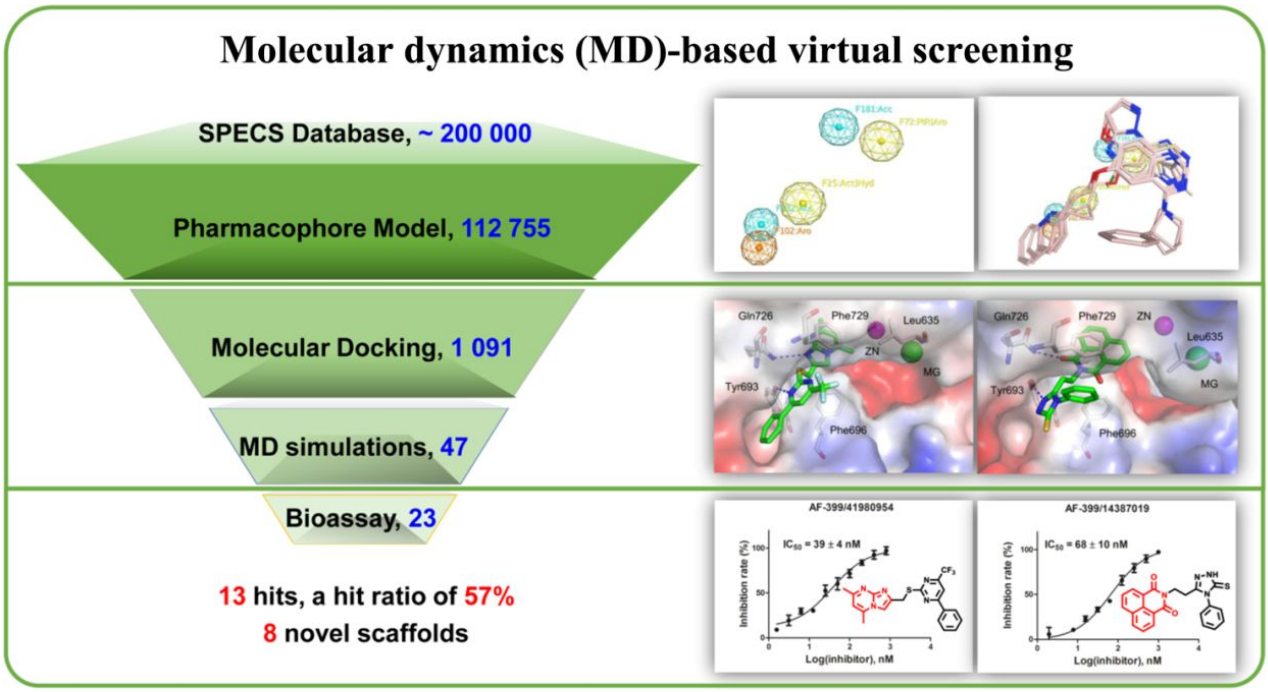

Figure 1. Flowchart of the molecular dynamics (MD)-based virtual screening procedure. The X-ray crystal structures of PDE10A in complex with the ligands (PDB ID: 3QPN, 3QPO, 3QPP, 5DH4, and 5DH5) were used to generated a 3D-pharmacophore model.

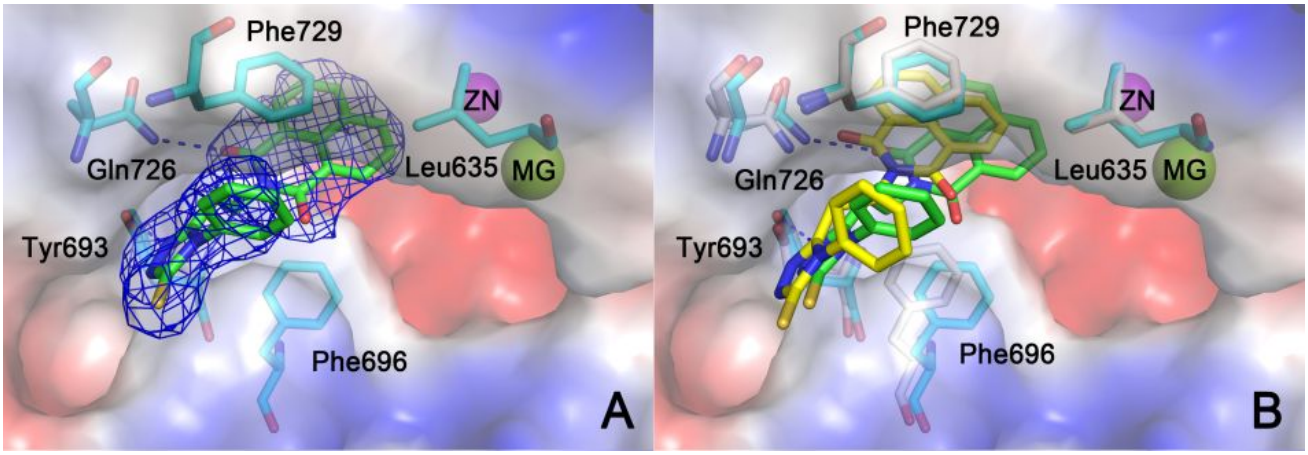

Figure 2. Binding of **AF-399/14387019** with PDE10. (A) Determined crystal structure of PDE10 in complex with **AF-399/14387019** (PDB ID: 6IJH). The 2Fo–Fc electron density is contoured in dark blue at 1.0 σ. (B) Alignment of the PDE10-**AF-399/14387019** crystal structure with the predicted binding mode. The predicted structure is depicted in silver and yellow, while the crystal structure is depicted in cyan and green.

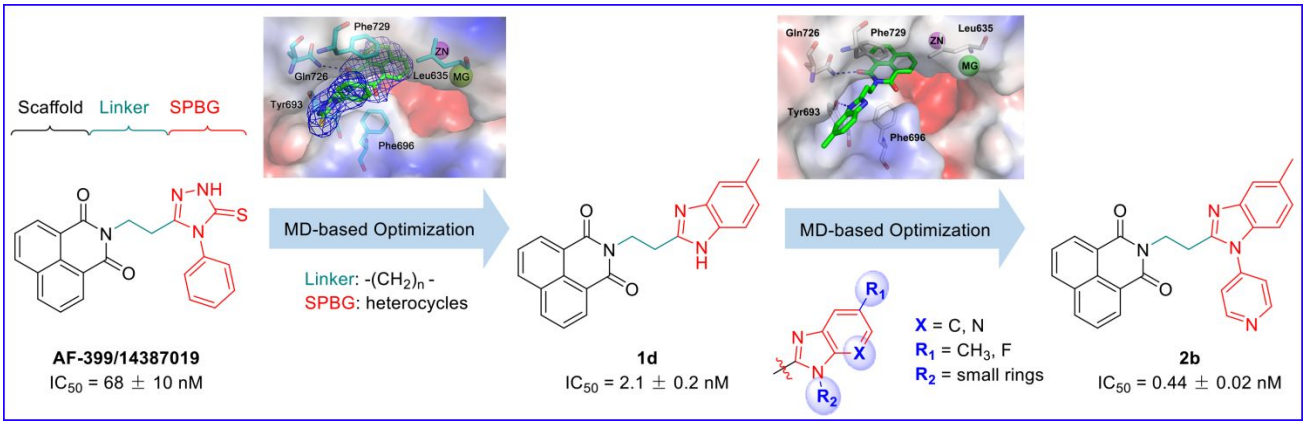

Figure 3. Two-round optimization based on molecular dynamics (MD) simulations. SPBG refers to a selective pocket binding group. The cocrystal structure of PDE10A with hit **AF-399/14387019** was used for MD simulation (PDB ID: 6IJH).

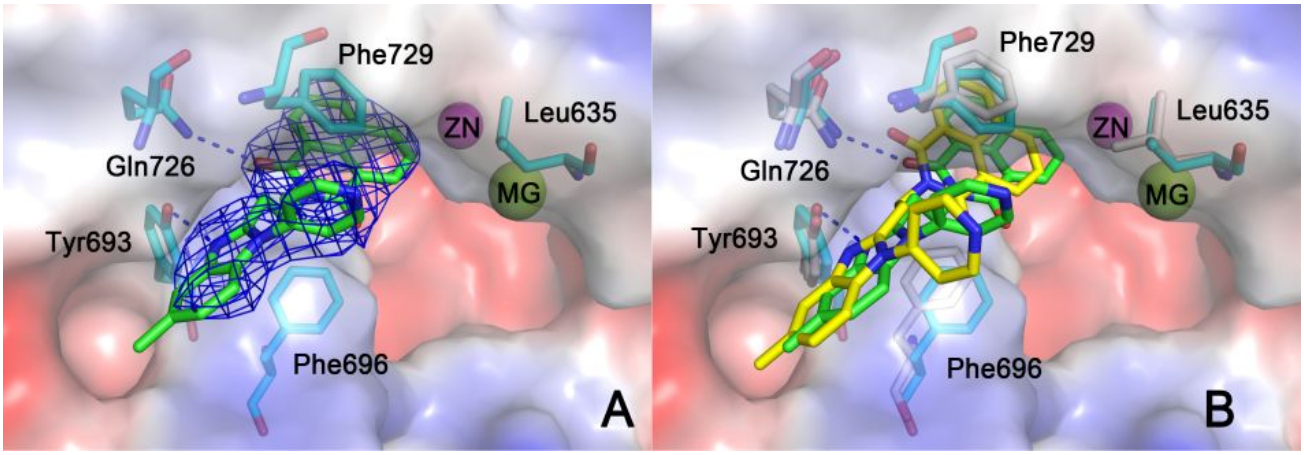

Figure 4. Binding of **2b** with PDE10A. (A) Cocrystal structure of PDE10A-**2b** (PDB ID: 6IJI). The 2Fo–Fc electron density is contoured in dark blue at 1.0 σ. (B) Alignment of the cocrystal structure of PDE10A-**2b** with the predicted binding mode. The predicted structure is depicted in silver and yellow, and the crystal structure is depicted in cyan and green.

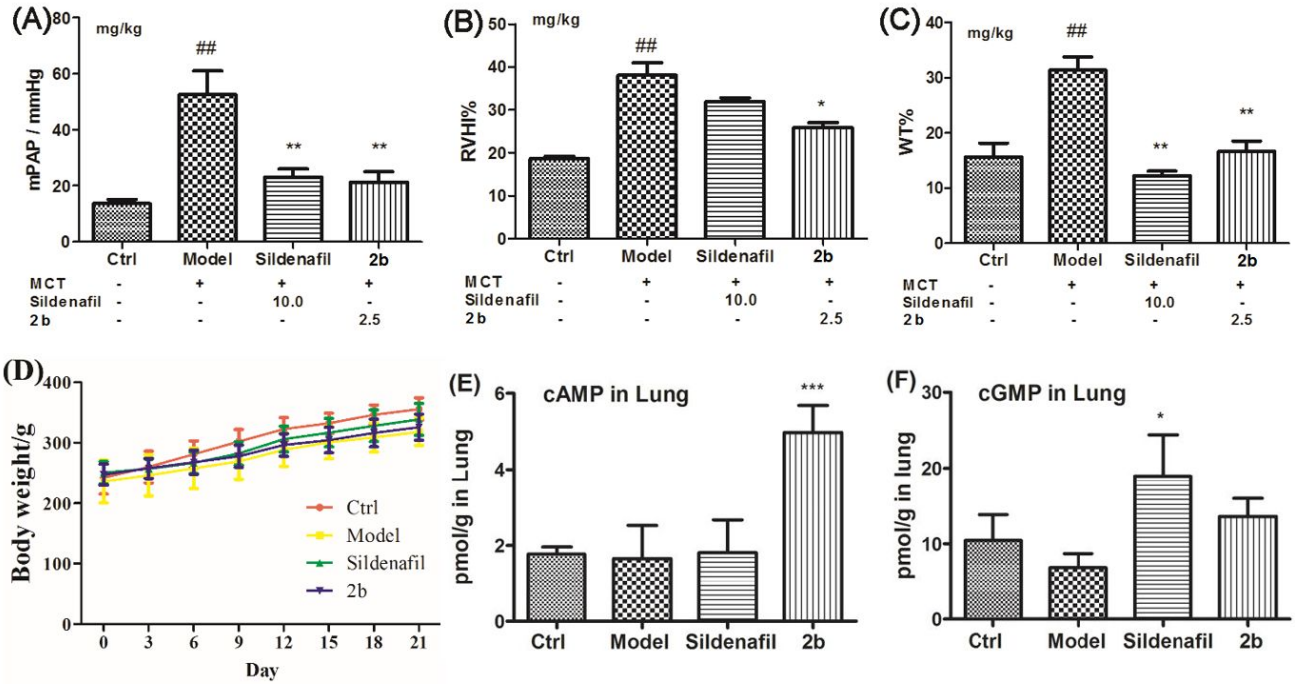

Figure 5. Effects of compound **2b** and sildenafil citrate on pulmonary arterial rat model *in vivo*. (A) The mean pulmonary artery pressure (mPAP) of different groups. (B) The right ventricle hypertrophy index (RVHI%) of different groups. (C) The wall thickness percentage (WT%) of different groups. Data are presented as means ± SD (n = 6−9 animals per group). (##) $p < 0.01$, (∗) $p < 0.05$, and (∗∗) $p < 0.01$ compared with the control group. (D) The body weight of different groups. (E) The concentration of cAMP in lung. (F) The concentration of cGMP in lung.

Table 1. The 1st Round of Optimization: Structures, Estimated Binding Free Energies, and Measured IC_{50} Values.

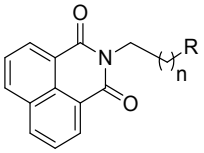

Compd.	n	R	Binding Free Energy (kcal/mol)	PDE10A2 IC_{50}[c] (nM)
AF-399/14387019	1	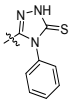	-29.17 ± 2.68[a] -30.90 ± 2.58[b]	68 ± 10
1a	1	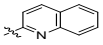	-32.60 ± 2.64[a] -35.11 ± 2.52[b]	20 ± 2
1b	1		-25.70 ± 3.36[a] -24.48 ± 2.91[b]	> 1000
1c	1	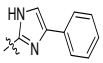	-31.54 ± 3.30[a] -34.27 ± 2.93[b]	10 ± 1
1d	1		-32.47 ± 2.82[a] -36.13 ± 2.27[b]	2.1 ± 0.2
1e	2	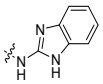	-32.69 ± 2.36[a] -36.63 ± 2.72[b]	>1000
1f	2	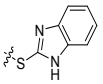	-34.06 ± 2.93[a] -36.94 ± 2.54[b]	182 ± 21

[a] Binding free energies are estimated by the MM/PBSA method. [b] Binding free energies are estimated by the MM/GBSA method. [c] Values are presented as the means ± SD of three experiments.

Table 2. The 2nd Round of Optimization: Structures, Estimated Binding Free Energies, and Measured IC_{50} Values.

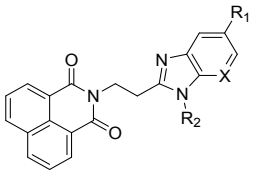

Compd.	X	R_1	R_2	Binding Free Energy (kcal/mol)	PDE10A2 IC_{50}[c] (nM)
2a	C	-F		-32.74 ± 4.01[a] -36.98 ± 2.76[b]	287 ± 29
2b	C	$-CH_3$		-37.71 ± 2.75[a] -40.54 ± 2.58[b]	0.44 ± 0.02
2c	C	$-CH_3$		-38.36 ± 3.25[a] -42.20 ± 2.89[b]	12 ± 1
2d	N	$-CH_3$		-38.42 ± 3.15[a] -39.34 ± 2.37[b]	23 ± 2
2e	N	$-CH_3$		-39.55 ± 3.01[a] -39.56 ± 2.46[b]	1.0 ± 0.2
2f	C	$-CH_3$		-40.22 ± 2.89[a] -43.30 ± 2.62[b]	0.76 ± 0.15

[a] Binding free energies are estimated by the MM/PBSA method. [b] Binding free energies are estimated by the MM/GBSA method. [c] Values are presented as the means ± SD of three experiments.

Table 3. Selectivity of Compound 2b across PDE Families

PDE catalytic domain	IC_{50} (nM)	Selectivity
PDE10A2 (449-770)	0.44	-
PDE1B (10-487)	>20 000	> 45 000-fold
PDE1C (2-634)	>20 000	> 45 000-fold
PDE2A (580-919)	>20 000	> 45 000-fold
PDE3A (679-1087)	>20 000	> 45 000-fold
PDE4D2 (86-413)	>20 000	> 45 000-fold
PDE5A1 (535-860)	>20 000	> 45 000-fold
PDE6C (1−858)	>20 000	> 45 000-fold
PDE7A1 (130-482)	>20 000	> 45 000-fold
PDE8A1 (480-820)	>20 000	> 45 000-fold
PDE9A2 (181-506)	>20 000	> 45 000-fold

Table 4 . The binding affinity of compound **2b** against various targets.[40-46]

ID	Target type	Target name	IC_{50}
1	Hormone receptor	Estrogen receptor ER_{α}	> 20 μM
2	Hormone receptor	Estrogen receptor ER_{β}	> 20 μM
3	Ion channel	hERG potassium channel	4.7 μM
4	Kinase	FGFR1	> 10 μM
5	Kinase	FGFR2	> 10 μM
6	Kinase	FGFR3	> 10 μM
7	Kinase	FGFR4	> 10 μM
8	Kinase	FLT3	> 10 μM
9	Kinase	ABL	> 10 μM
10	Kinase	Aurora A	> 10 μM
11	Kinase	Aurora B	> 10 μM
12	Kinase	PLK1	> 10 μM
13	Kinase	EGFR	> 10 μM
14	Kinase	ZAK	> 10 μM
15	Enzyme	BRD4	> 10 μM
16	Enzyme	COX2	> 10 μM
17	Enzyme	HDAC1	> 10 μM
18	Enzyme	HDAC6	> 10 μM
19	Enzyme	AChE	> 20 μM
20	Enzyme	BChE	> 20 μM

[40-46] References for the ligand profiling used.

Table 5. Pharmacokinetic Profile of Compound 2b in Rats.

	$t_{1/2}$	T_{max}	C_{max}	$AUC_{(0-t)}$	$AUC_{(0-\infty)}$	CL	$MRT_{(0-t)}$	Vss
	h	h	ng/mL	h*ng/mL	h*ng/mL	mL/h/kg	h	L/kg
data	0.58	0.083	3500.87	1097.38	1098.64	2336.62	0.21	0.51
SD	±0.02	±0.001	±726.12	±214.95	±215.35	±470.38	±0.02	±0.11

Scheme 1. General Procedures Used to Synthesize Compounds **1a-1b.** [a]

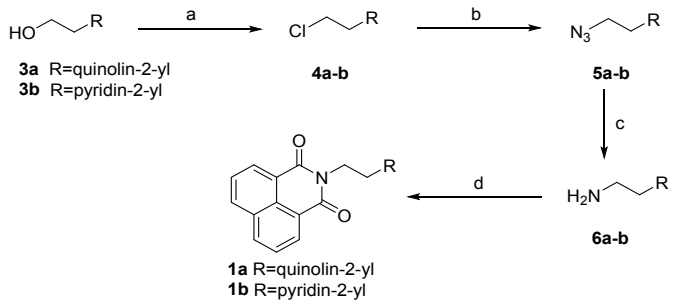

[a]Reagents and conditions: (a) $SOCl_2$, CH_2Cl_2, rt, 1 h (65-94%); (b) NaN_3, DMF, 70 °C, 12 h (79-86%); (c) H_2, Pd/C, EtOH, 1,4-dioxane , rt, 4 h (91-92%); (d) 1H,3H-benzo[de]isochromene-1,3-dione, EtOH, reflux, 3 h (83-85%).

Scheme 2. General Procedures Used to Synthesize Compounds **1c-1d.** [a]

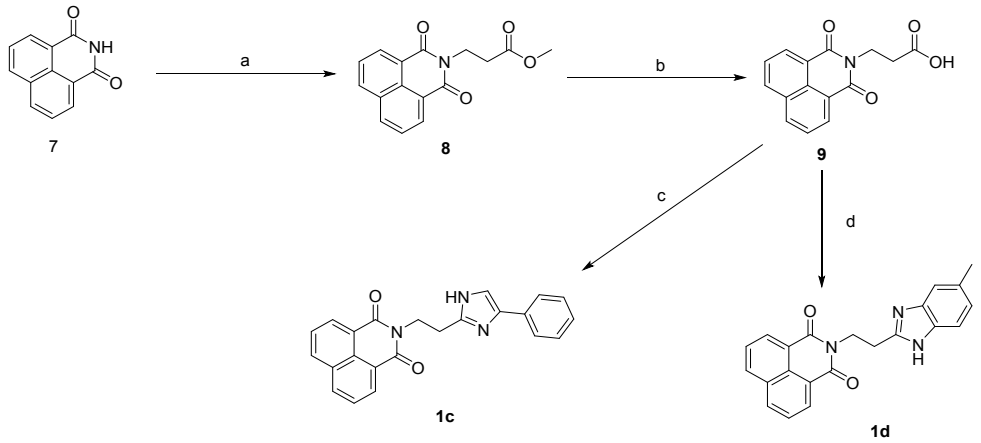

[a]Reagents and conditions: (a) 1,4-dioxane, 25 °C, reflux, 4 h (52-55%); (b) H_2, $Pd(OH)_2/C$, EtOH, 6 h (83-89%); (c) (i) **9**, HATU, DIPEA, CH_2Cl_2, 12 h; (ii) AcOH, 90 °C, 12 h (72-78% over two steps); (d) RNH_2, $Pd_2(dba)_3$, PhMe, Cs_2CO_3, BINAP, 110 °C, 24 h (52-65%); (e) H_2, $Pd(OH)_2/C$, EtOH, 6 h (50-81%); (f) (i) **9**, HATU, DIPEA, CH_2Cl_2, 12 h; (ii) AcOH, 90 °C, 12 h (50-81% over two steps).

Scheme 3. General Procedures Used to Synthesize Compounds **1e-1f.** [a]

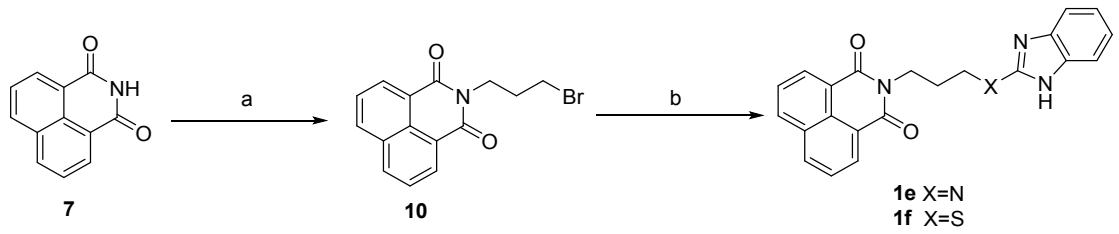

[a]Reagents and conditions: (a) 1,3-dibromopropane, K_2CO_3, MeCN, reflux, 12 h (90%); (b) 1H-benzo[d]imidazol-2-amine or 1H-benzo[d]imidazole-2-thiol, NaH, DMF, 0 °C, 2 h (75-84%).

Scheme 4. General Procedure Used to Synthesize Compounds **2a-2f.** [a]

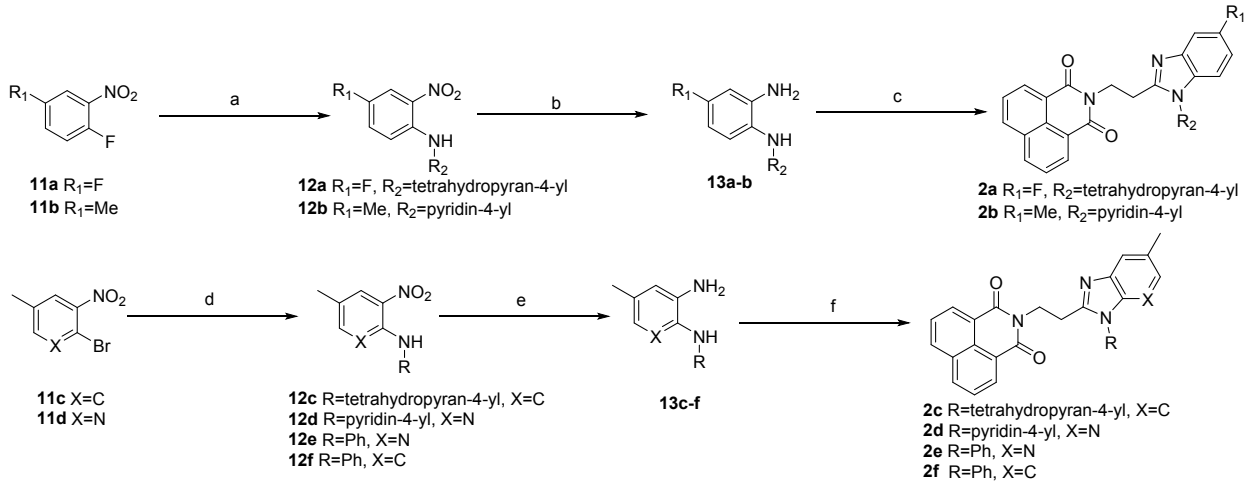

[a]Reagents and conditions: (a) 1,4-dioxane, reflux, 4 h (52-55%); (b) H_2, $Pd(OH)_2/C$, EtOH, 6 h (83-89%); (c) (i) **9**, HATU, DIPEA, CH_2Cl_2, 12 h; (ii) AcOH, 90 °C, 12 h (72-78% over two steps); (d) RNH_2, $Pd_2(dba)_3$, PhMe, Cs_2CO_3, BINAP, 110 °C, 24 h (52-65%); (e) H_2, $Pd(OH)_2/C$, EtOH, 6 h (50-81%); (f) (i) **9**, HATU, DIPEA, CH_2Cl_2, 12 h; (ii) AcOH, 90 °C, 12 h (50-81% over two steps).

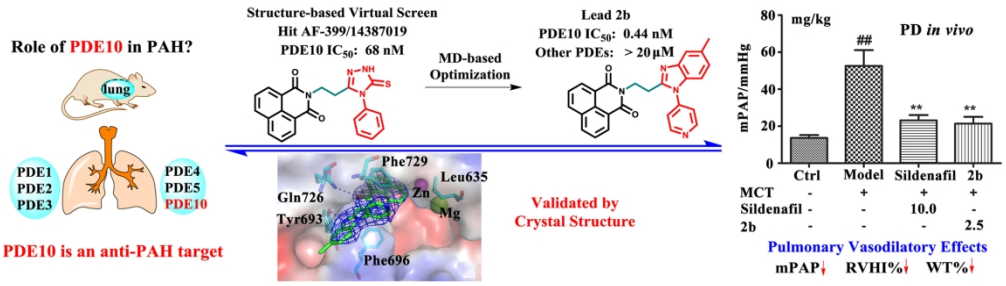

Table of content graphic

197x54mm (300 x 300 DPI)